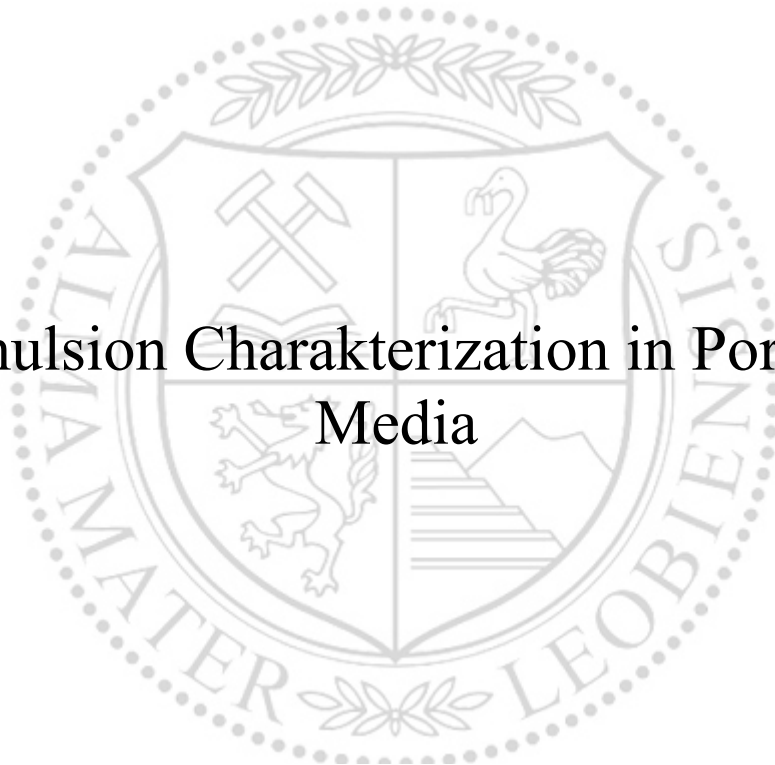




Chair of Reservoir Engineering

Master's Thesis

Emulsion Charakterization in Porous  
Media



Bianca Brandstätter

Master Thesis 2020/21

Supervisor: Univ.-Prof. Dipl.-Phys. Dr.rer.nat. Holger Ott

Co-supervisor: Dipl. Ing. Ahmad Kharrat

# Emulsion Characterization in Porous Media

*To my parents, brothers and friends.*

## **Declaration**

I hereby declare that except where specific reference is made to the work of others, the contents of this dissertation are original and have not been published elsewhere. This dissertation is the outcome of my own work using only cited literature.

## **Erklärung**

Hiermit erkläre ich, dass der Inhalt dieser Dissertation, sofern nicht ausdrücklich auf die Arbeit Dritter Bezug genommen wird, ursprünglich ist und nicht an anderer Stelle veröffentlicht wurde. Diese Dissertation ist das Ergebnis meiner eigenen Arbeit mit nur zitierter Literatur.



---

Name, 02 June 2021

## Acknowledgments

I would like to thank Prof. Holger Ott for supervising and advising me throughout my studies, sharing his ideas and knowledge with me and broadening my horizon.

A special thank you to Ahmad Kharrat, who always guided and mentored me.

Furthermore, I want to thank my coworkers and colleagues Pit Arnold, Peyman Nazifi, Michael Koopmans, Horst Resch and Bettina Matzer for supporting me.

Last but not least, I would like to thank my family, friends and boyfriend, who always had my back and made me smile.

## Abstract

The controlled formation of emulsions plays a significant part in numerous sectors, with one of them being the oil and gas industry. During the tertiary stage of oil production, also called enhanced oil recovery, gas injections, chemical- and thermal methods come into application and which can achieve an ultimate recovery of 30 to 60%. It targets the residual oil and therefore improves the microscopic sweep efficiency by mobility control, wettability alteration, viscosity and interfacial tension reduction. This thesis focuses on surfactant flooding, which falls under the chemical methods category and covers the investigation and characterization of emulsions by utilizing fluorescent imaging techniques.

The surfactant used was the Ernodett J13131 and was mixed with a cosolvent, 2-butanol and distilled water. The salinity was varied by changing the amount of sodium chloride added. Three salinity concentrations were investigated: 1% (w/v), 2% (w/v), 4% (w/v). For the fluorescent imaging, fluorescein sodium salt was added and the oleic phase was resembled by decane.

Phase behaviors were performed to state the influence of the fluorescein salt on the surfactant. Therefore, two test groups were established, which did not show any visual differences between them.

To detect the ideal amount of fluorescein salt and to find a relationship between concentration and the mean grey value, a fluorescent intensity analysis was performed by injecting eight different solutions. With the base being distilled water and varying fluorescent dye concentration (2, 5, 10, 20, 50, 80, 100, 300 mg/l). 100 mg/l was chosen to be the best option for the displacement experiments. A linear relationship was found, where 100% results in a pure aqueous phase and 0% to a pure oleic phase.

The displacement behaviors were performed in a fully decane saturated microfluidic chip, which was then displaced by a 1, 2 and 4% NaCl surfactant solution with 100 mg/l added fluorescein salt. It was observed that the optimum range must lay between 2 and 4% NaCl while the 2% solution performed the best out of all experiments.

Additionally, interfacial tension measurements were performed by using the pendant drop method and spinning drop tensiometer. However, no precise results could be stated, which need further investigation.

## Zusammenfassung

Die kontrollierte Bildung von Emulsionen spielt in zahlreichen Branchen eine bedeutende Rolle, unter anderem in der Öl- und Gasindustrie. Während der tertiären Phase der Ölförderung, auch Enhanced Oil Recovery genannt, werden Gasinjektionen, chemische und thermische Verfahren eingesetzt um eine Endausbeute von 30 bis 60 % zu erreichen. Diese Methoden zielen auf das verbliebene Öl ab und verbessern damit die mikroskopische Durchlauffeffizienz durch Mobilitätskontrolle, Benetzbarkeitsänderung, Viskositäts- und Grenzflächenspannungsreduzierung. Im Rahmen dieser Thesis werden Surfactant Injektion analysiert, mit Fokus auf die Charakterisierung von Emulsionen unter Verwendung fluoreszierender Bildgebungsverfahren.

Die Untersuchungen wurden mit dem Surfactant Ernodett J13131 durchgeführt und mit 2-Butanol, als Co-Surfactant, und destillierten Wasser gemischt. Der Salzgehalt wurde durch Ändern der zugegebenen Natriumchloridmenge variiert. Drei Salinitätskonzentrationen wurden untersucht: 1% (w/v), 2% (w/v), 4% (w/v). Für die fluoreszierende Bildgebung wurde Fluorescein-Natriumsalz zugegeben und Dekan als Ölphase benutzt.

Phasenverhalten wurde durchgeführt, um den Einfluss des Fluoresceinsalzes auf den Surfactant zu bestimmen. Zwei Testgruppen mit jeweils drei Lösungen wurden verglichen, welche keine optisch sichtbaren Unterschiede aufwiesen.

Um die ideale Menge an Fluoresceinsalz zu ermitteln und eine Beziehung zwischen der Konzentration und dem mittleren Grauwert zu finden, wurde eine Fluoreszenzintensitätsanalyse durchgeführt, indem acht verschiedene Lösungen injiziert wurden. Mit destilliertem Wasser und unterschiedlicher Konzentration des Fluoreszenzfarbstoffes (2, 5, 10, 20, 50, 80, 100, 300 mg/l). Die Lösung mit 100 mg/l wies die besten Eigenschaften auf und wurde daher für die Verdrängungsexperimente ausgewählt. Weiters, konnte ein linearer Zusammenhang beobachtet werden zwischen fluoreszierender Intensität und Menge der wässrigen Lösung.

Das Verdrängungsverhalten wurde in einem vollständig mit Dekan gesättigten Mikrofluidik-Chip durchgeführt, welcher dann durch eine 1, 2 und 4 prozentige NaCl-Surfactant-Lösung, mit 100 mg/l zugesetztem Fluoresceinsalz, geflutet wurde. Es wurde beobachtet, dass der optimale Bereich zwischen 2 und 4% NaCl liegt, während die 2%ige Lösung am nächsten zum Optimum kommt.

Zusätzlich wurden Grenzflächenspannungsmessungen unter Verwendung der Pendant-Drop-Methode und des Spinning-Drop-Tensiometers durchgeführt. Es konnten jedoch keine genauen

Ergebnisse angegeben werden, jedoch konnte eine Grenzflächenspannungsreduzierung beobachtet werden.



## Table of Contents

Declaration.....	iii
Erklärung .....	iii
Acknowledgments .....	iv
Abstract.....	v
Zusammenfassung .....	vi
Chapter 1.....	19
Introduction.....	19
1.1 Background and Context.....	19
1.2 Scope and Objectives .....	20
Chapter 2.....	21
State of the Art.....	21
2.1 Enhanced Oil Recovery .....	21
2.2 Surfactant & Emulsion.....	22
2.3 Microfluidics in Porous Media .....	29
Chapter 3.....	33
Experimental Utensils.....	33
3.1 Apparatus .....	33
3.2 Chemicals.....	35
3.3 Programs .....	36
Chapter 4.....	37
Experimental Setup, Methodology & Analysis .....	37
4.1 Microfluidic Displacement .....	37
4.2 Characterization of Fluid System.....	42
Chapter 5.....	47
Results and Discussion .....	47
5.1 Microfluidic Displacement .....	48
5.2 Characterization of Fluid System.....	66
Chapter 6.....	69
Conclusion .....	69
6.1 Summary .....	69
6.2 Future Work.....	70
Chapter 7.....	73
References.....	73
Appendix Title .....	A-1



## List of Figures

Figure 2-1 – Left: structure of a surfactant; Right: micelle formation.....	23
Figure 2-2 – Surfactant concentration below and above CMC.....	24
Figure 2-3 – Surfactant concentration vs. surfactant monomer concentration (left) and vs. IFT (right) -based on (Lake et al. 2014) .....	24
Figure 2-4 – Winsor Classification for Emulsions - based on (Winsor 1948).....	25
Figure 2-5 – Anionic surfactant at the oil-brine interface (Buijse et al. 2012) .....	26
Figure 2-6 – Curvature for emulsions at different salinities(Buijse et al. 2012).....	26
Figure 2-7 – Ternary Diagram for Phase Behavior Experiments with different Salinities (Sheng 2011) .....	27
Figure 2-8 – Schematical Sketch of a pendant drop measurement .....	28
Figure 2-9 – Pendant drop – geometrical variables (Zeppieri et al. 2001).....	28
Figure 2-10 – Spinning drop principle (Dataphysics).....	29
Figure 2-11 – T-junction with different flow regimes: geometry (a), squeezing regime (b), dripping regime (c), jetting regime (d) (Liu et al. 2020).....	30
Figure 2-12 – Emulsion formation for an n-decan filled dead-end pore for under-optimum and over-optimum salinities and varying injection rates (Broens and Unsal 2018) .....	31
Figure 3-1 – EOR Physical Rock Network – Microfluidic Chip (Micronit) .....	34
Figure 4-1 – Experimental Setup – Microfluidic Displacement .....	38
Figure 4-2 – Closeup of micromodel structure with injection direction from left to right .....	39
Figure 4-3 – Settings for fluorescent image capturing in LAS X .....	40
Figure 4-4 – RGB color scheme for black (left) and white (right) .....	41
Figure 4-5 – Selection mask for pore (left) and grain area (right).....	42
Figure 4-6 – Experimental Setup – Pendant Drop .....	43
Figure 4-7 – – Experimental Setup – Spinning Drop .....	44
Figure 5-1 – Fluorescent Intensity Analysis Results .....	48
Figure 5-2 – Fluorescent Intensity Analysis: $\Delta$ Mean vs. Fluorescein Salt Concentration [mg/l] .....	50
Figure 5-3 – Fluorescent Intensity Analysis: $\Delta$ Mean vs. Fluorescein Salt Concentration [%] .....	50
Figure 5-4 – Micromodeled with labeled stages (red) .....	51
Figure 5-5 – Selected Stages.....	51
Figure 5-6 – Experiment 1.1 (1% NaCl) – Stage 06.....	52
Figure 5-7 – Experiment 1.2 (2% NaCl) – Stage 06.....	53
Figure 5-8 – Experiment 1.3 (4% NaCl) – Stage 06.....	53
Figure 5-9 – Experiment 1.1 (1% NaCl) – Stage 12.....	54
Figure 5-10 – Experiment 1.2 (2% NaCl) – Stage 12.....	55
Figure 5-11 – Experiment 1.3 (4% NaCl) – Stage 12.....	55
Figure 5-12 – Experiment 1.1 (1% NaCl) – Stage 28.....	56
Figure 5-13 – Experiment 1.2 (2% NaCl) – Stage 28.....	56
Figure 5-14 – Experiment 1.2 (2% NaCl) – Stage 28 Zoom In – dead-end pore .....	57
Figure 5-15 – Experiment 1.3 (4% NaCl) – Stage 28.....	57
Figure 5-16 – Experiment 1.2 (2% NaCl) – Stage 06 – Mixing Analysis .....	59
Figure 5-17 – Experiment 1.2 (2% NaCl) – Stage 12 – Mixing Analysis .....	60
Figure 5-18 – Experiment 1.2 (2% NaCl) – Stage 28 – Mixing Analysis .....	60
Figure 5-19 – Experiment 1.2 (2% NaCl) – Stage 28 Zoom in – Mixing analysis.....	61
Figure 5-20 – Experiment 1.3 (4% NaCl) – Stage 06 – Mixing Analysis .....	61
Figure 5-21 – Experiment 1.3 (4% NaCl) – Stage 12 – Mixing Analysis .....	62
Figure 5-22 – Experiment 1.3 (4% NaCl) – Stage 06 – Mixing Analysis .....	62
Figure 5-23 – Experiment 1.1 (1% NaCl) – Merged image: fluorescent ILL (top); normal ILL (bottom) .....	63
Figure 5-24 – Experiment 1.2 (2% NaCl) – Merged image: fluorescent ILL (top); normal ILL (bottom) .....	64

Figure 5-25 – Experiment 1.3 (4% NaCl) – Merged image: fluorescent ILL (top); normal ILL (bottom) .....	65
Figure 5-26 – Experiment 3.1 (1% NaCl).....	66
Figure 5-27 – Experiment 3.2 (2% NaCl) – Timeline from left to right.....	66
Figure 5-28 – Experiment 4.2 (2% NaCl): 1000 rpm, 25.7°C .....	67
Figure 5-29 – Experiment 4.3 – Attempts to measure IFT: 300 rpm, 25.9°C(left); 4000 rpm, 25.9°C (middle); 4000 rpm, 30°C (right).....	67
Figure 5-30 – Phase Behavior Results: experiment 5.1 (left) to 5.6 (right).....	68
Figure 7-1 – Experiment 1.1 (1% NaCl) – Stage 06 – Mixing Analysis .....	A-3
Figure 7-2 – Experiment 1.1 (1% NaCl) – Stage 12 – Mixing Analysis .....	A-3

## List of Tables

Table 1 – Dimensions of Physical Rock Network - Microfluidic Chip (Micronit) .....	34
Table 2 – Chemicals.....	35
Table 3 – Solution for Fluorescent Displacement Experiments.....	37
Table 4 – Solutions for Fluorescent Intensity Analysis .....	40
Table 5 – Solutions for Pendant Drop and Spinning Drop Experiments .....	43
Table 6 – Solutions for Phase Behavior Experiments.....	44
Table 7 – Results Fluorescent Intensity Analysis for Experiment 2.1 – 2.4.....	49
Table 8 – Results Fluorescent Intensity Analysis for Experiment 2.5 – 2.8.....	49
Table 9 – List of all Experiments.....	A-1



## Nomenclature

$E$	Ultimate displacement efficiency	-
$E_D$	Microscopic displacement efficiency	-
$E_V$	Macroscopic displacement efficiency	-
$M$	Mobility ratio	-
$\lambda$	Phase mobility	-
$k_r$	Relative permeability	-
$\mu$	Viscosity	[cP]
$N_C$	Capillary number	-
$F_V$	Viscous force	-
$F_C$	Capillary force	-
$v$	Pore flow velocity	[m/s]
$\sigma$	Interfacial tension	[mN/m]
$S_{oi}$	Initial oil in place saturation	-
$S_{or}$	Residual oil saturation	-
$R$	Radius	[m]
$\omega$	Rotational speed	[1/s]
$\rho$	Density	[kg/m <sup>3</sup> ]
$g$	Gravitational acceleration	[m/s <sup>2</sup> ]



## Abbreviations

EOR	Enhanced Oil Recovery
IFT	Interfacial Tension
CMC	Critical Micelle Concentration
WR	Winsor Ratio
DI-W	Distilled water
RGB	Red, Green, Blue



# Chapter 1

## Introduction

Emulsions are a common occurrence in daily life. They can be found in milk and dairy products, pharmaceutical products, cosmetics and many more. One application, which is the primary topic of this thesis, is emulsions in enhanced oil recovery (EOR).

After primary and secondary oil production may become not economical anymore and EOR comes into play. Surfactant flooding is one type of EOR and falls under the category of chemical methods. It goes hand in hand with emulsion formation, reducing the interfacial tension (IFT) between oil and aqueous phase and enhancing mobility.

Salinity is one factor that affects emulsions and can either lead to an under-optimum, optimum, or over-optimum state. Microfluidic chips help to investigate emulsions in a semi two-dimensional way and show the effects of changing salinity on the emulsion formation process.

### 1.1 Background and Context

In general oil and water are not miscible due to the high IFT. However, this can be improved by emulsions, which are formed during surfactant floods. And even though this thesis only focuses on the displacement of oil, an improved understanding of these subjects could be also for use in other scientific areas.

Previously, complex displacement processes with altering compositions in microfluidic devices, as well as IFT measurements using different methods, were performed in (Mostafa Borj 2017), (Ahmad Kharrat 2018), (Pit Arnold 2018) and (Ott et al. 2020). This thesis should add to those findings by investigating displacement processes in surfactant flooding.

## 1.2 Scope and Objectives

In this thesis, the formation of emulsions with varying salt concentrations is investigated using a microfluidic chip with a porous network structure. Decane acts as the oleic phase and is displaced by three different surfactant solutions with salt concentrations of 1, 2 and 4 (w/v)%. By adding fluorescein dye to the aqueous phase, the visibility of the mixing is enhanced and the processes can be observed in an even better way.

This thesis aims to give a better understanding of the emulsion formation processes, its displacement behavior and to give a basis for future work by investigating the relationship between fluorescein salt concentration and fluorescence intensity.

# Chapter 2

## State of the Art

The following chapter gives a brief introduction about EOR, surfactants and emulsions and a short overview of current projects.

### 2.1 Enhanced Oil Recovery

An oil field's production can be split into three stages: primary, secondary and tertiary. The well needs no additional support during primary production and the fluids are produced utilizing the natural drive mechanisms, like water drive, gas drive and gas cap drive. For secondary production, additional support is needed in the form of either gas or water injection to keep the reservoir pressure at an economic level. The tertiary stage, also called enhanced oil recovery, uses a variety of methods and targets the reduction of the remaining oil in the reservoir by mobility control (See 2.1.1), IFT reduction (See 2.1.2) and wettability alteration. Therefore, it improves the microscopic sweep efficiency (See (2.1) and (2.2)). Where  $E$  stands for the ultimate-,  $E_D$  for the microscopic- and  $E_V$  for the macroscopic/volumetric- displacement efficiency.  $S_{oi}$  describes the initial oil in place and  $S_{or}$  the residual oil (Green and Willhite 2008).

$$E = E_D \times E_V \quad (2.1)$$

$$E_D = \frac{S_{oi} - S_{or}}{S_{oi}} \quad (2.2)$$

Surfactant flooding falls under chemical EOR methods and is the main topic of this master thesis.

### 2.1.1 Mobility control

As mentioned before, mobility is an important objective in EOR and is defined as the capability of an immiscible fluid to displace oil (Donaldson and Alam 2008). Mobility can be controlled by either lowering the viscosity of the displaced fluid, in this relationship the oleic phase, or by reducing the relative permeability of the displaced fluid. This becomes more obvious when looking at equation (2.3), where  $M$  is the mobility ratio,  $\lambda$  the phase mobility,  $\mu$  the viscosity,  $k_r$  the relative permeability and the index  $d$  for the displaced phase and  $D$  for the displacing phase. The mobility ratio is favorable, if it is smaller than one, otherwise viscous or capillary fingering can be expected (Sheng 2011).

$$M = \frac{\lambda_D}{\lambda_d} = \frac{\frac{k_{r,d}}{\mu_d}}{\frac{k_{r,D}}{\mu_D}} = \frac{k_{r,d} \times \mu_D}{k_{r,D} \times \mu_d} \quad (2.3)$$

Surfactants alone are not capable of altering the mobility ratio. However, a combination of surfactant and polymer flooding can simultaneously lower the IFT and increase water viscosity (Sun et al. 2020).

### 2.1.2 Capillary number

The capillary number is one of the main targets in surfactant flooding. It can indicate if fluid is trapped or mobile and is described by the ratio of viscous forces ( $F_v$ ) over capillary forces ( $F_c$ ). The viscous forces are the dragging forces which are mobilizing the displaced phase and the capillary forces trap them. Therefore, it is favorable if the viscous forces are greater than the capillary forces, which means a capillary number greater than one is to favor. In equation (2.4),  $v$  stands for the pore flow velocity of the displacing fluid,  $\mu$  for the viscosity of the displacing fluid and  $\sigma$  for the IFT between the displacing and the displaced phase (Sheng 2011).

$$N_c = \frac{F_v}{F_c} = \frac{v \times \mu}{\sigma} \quad (2.4)$$

The implementation of surfactant flooding increases the capillary number by decreasing the IFT tension between oil and water and is described in more detail in the second part of this chapter.

## 2.2 Surfactant & Emulsion

Emulsions can be found in everyday life and have a wide variety of applications. They are generally described as a colloidal dispersion of one immiscible liquid in another liquid (Gold

2019). We can find applications in the food industry, where emulsions enhance the stability and quality of foods (Guzey and McClements 2006), the pharmaceutical industry as creams or drug delivery systems (Khan 2011) and most interesting for this thesis: the oil and gas industry.

Emulsions are typically unstable and therefore, emulsifiers or surfactants have to be added to reduce the IFT tension. Surfactants are surface-active agents with a hydrophilic head and a hydrophobic/lipophilic chain (see Figure 2-1) (Schramm 2000). The hydrophilic head dissolves in the aqueous solution, while the lipophilic part dissolves in the oleic phase. They can be sorted into different groups, determined by the polarity of the head: anionic, cationic, nonionic and zwitterionic. Anionic surfactants are the most widely used in the oil and gas industry since they are unlikely to be absorbed by sandstone rocks, which are negatively charged (Azam et al. 2013). Nonionic surfactants are usually used as cosurfactants to improve the system phase behavior and due to their high salinity tolerance (Sheng 2011). However, the IFT reduction is insufficient and therefore, it is preferred to use a mixture of anionic and cationic surfactants for this purpose. On the other hand, Cationic surfactants cannot be used in sandstone reservoirs since they are highly absorbed and find their application in carbonate reservoirs with low silicone composition (Ma et al. 2013), where they might change the system from an oil-wet to a much more preferred water-wet system. Zwitterionic, also amphoteric, surfactants are pretty expensive compared to other types, but they are superior while dealing with high temperatures and high salinities (Sheng 2011).



Figure 2-1 – Left: structure of a surfactant; Right: micelle formation

### Critical Micelle Concentration:

An essential key parameter is the critical micelle concentration (CMC), where the surfactants (monomers) spontaneously form aggregates (micelles). When surfactants are first introduced into the system, they accumulate at the interface. They reduce the system's free energy by reducing the surface energy (product of area and surface tension) and reducing the exposure of the lipophilic parts to the aqueous phase. Till the CMC is reached, adding surfactants results in a sharp decrease of IFT (see Figure 2-2 and Figure 2-3) (Sheng 2011). The typical range for the CMC is relatively low and about  $10^{-5}$  to  $10^{-4}$  mol/L (Green and Willhite 2008).

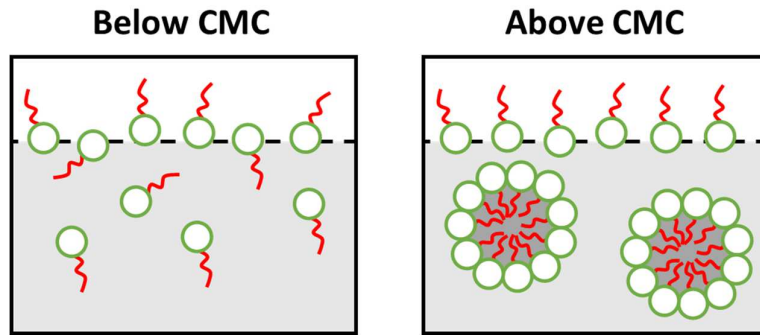


Figure 2-2 – Surfactant concentration below and above CMC

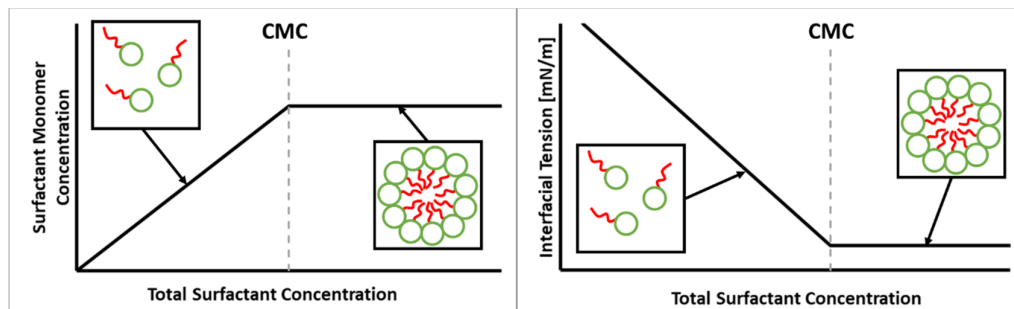


Figure 2-3 – Surfactant concentration vs. surfactant monomer concentration (left) and vs. IFT (right) - based on (Lake et al. 2014)

### Winsor Classification:

There are different types of emulsions: water-in-oil (W/O), oil-in-water (O/W), a transition between those two and more complex systems like water-in-oil-in-water (W/O/W). Winsor type I microemulsions are oil-in-water (O/W) emulsions, where the oil is in the middle of the micelle. Winsor Type II is defined as water-in-oil (W/O), which is the other way around. This occurs if the surfactant is strongly hydrophobic and remains in the oleic phase. Winsor Type III is defined as a transition between those two (see Figure 2-4) and can be accomplished by changing the temperature or adding cosolvents (Sweeta Akbari 2018; Schramm 2000).

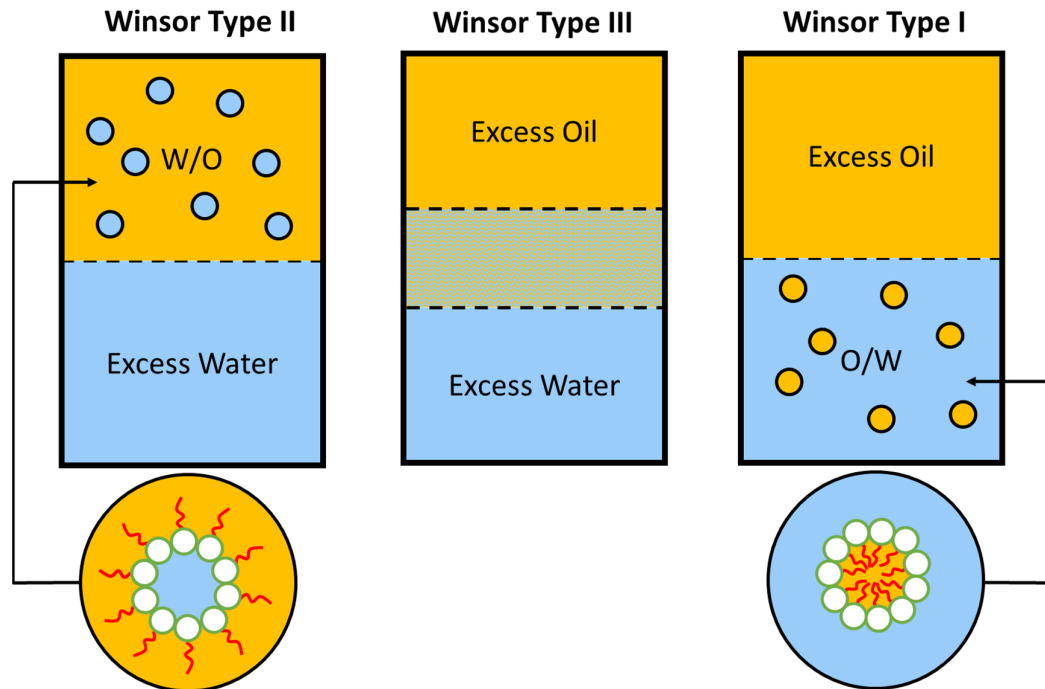


Figure 2-4 – Winsor Classification for Emulsions - based on (Winsor 1948)

Winsor Type III emulsions have an ultra-low IFT and are therefore preferred in the oil and gas industry (Nordiyana et al. 2016). Type III can increase the capillary number (See 2.1.2) and the displacement efficiency of crude oil (Schramm 2000).

#### Winsor Ratio and Salinity:

Another factor that influences emulsions immensely is the salinity of the aqueous phase, which is expected to be high in a petroleum reservoir containing water. One method to describe this is the Winsor Ratio concept. The attractive forces between the hydrophilic head and the aqueous phase ( $E_{\text{Head-Brine}}$ ) as well as the attractive forces between the lipophilic tail and the oleic phase ( $E_{\text{Tail-Oil}}$ ) (See Figure 2-5), can decrease the repulsive forces and thus lowering the IFT between the brine and the oleic phase. The Winsor Ratio (WR) is the ratio between those forces (See (2.5)) and an ultralow IFT can be achieved if both forces are large and equal, which results in a WR equal one as an optimum. However, it is important to note that the Winsor Ratio concept is not entirely correct because there is no physical interpretation for the attractive forces, even if it is often used due to its simplicity (Buijse et al. 2012).

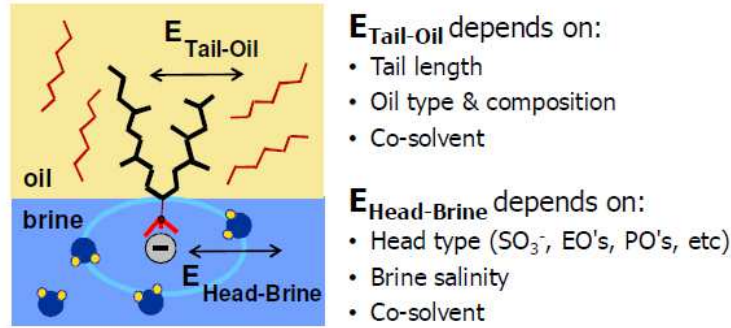


Figure 2-5 – Anionic surfactant at the oil-brine interface (Buijse et al. 2012)

$$WR = \frac{E_{Tail-oil}}{E_{Head-Brine}} \quad (2.5)$$

Ionic surfactants interact with the ions in the brine and are therefore dependent on the salinity. At low salinity, we expect an under-optimum, oil-in-water (O/W), emulsion and at high salinity an over optimum, water-in-oil (W/O), emulsion. We speak from optimum salinity if a third phase, a so-called microemulsion, is formed, which contains equal parts of oil and brine and exhibits the lowest possible IFT (Al-Yaari et al. 2015).

Another method to describe emulsions can be done by considering the curvature of the interfacial film, which results from the shielding effect of the head. At a WR smaller than one, low salinity, the surfactant head has minimal shielding. This results in repulsion between the heads and forms an oil-in-water emulsion. At WR greater one, high salinity, the opposite effect can be observed, where the head shielding is strong. At the optimum salinity, no curvature is formed and a microemulsion formation can be observed (See Figure 2-6) (Buijse et al. 2012).

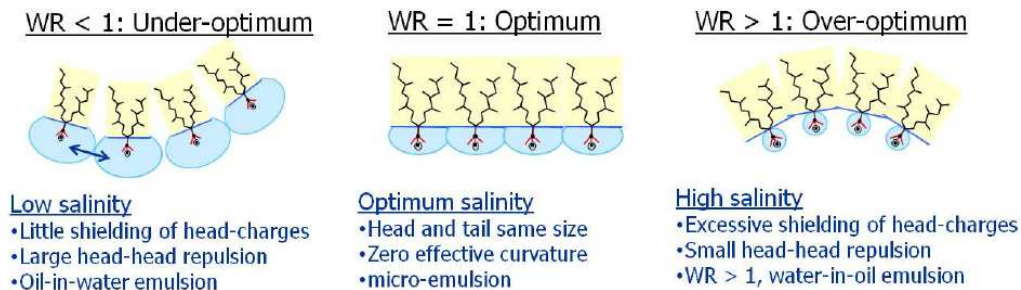


Figure 2-6 – Curvature for emulsions at different salinities (Buijse et al. 2012)

## 2.2.1 Phase Behavior

A common way to find optimum conditions is to conduct phase behavior experiments. The study of phase behavior is a complex topic since it is dependent on many factors, like surfactant type and concentration, cosurfactants, hydrocarbons, brine and temperature. Although phase behavior experiments are static and may not represent the dynamic (fluids contact at flow conditions) behavior completely, they can give a visual indication about the optimum salinity and the type of emulsion which has been formed (Green and Willhite 2008). Additionally, they can be described and quantified using ternary diagrams, which can be seen in Figure 2-7.

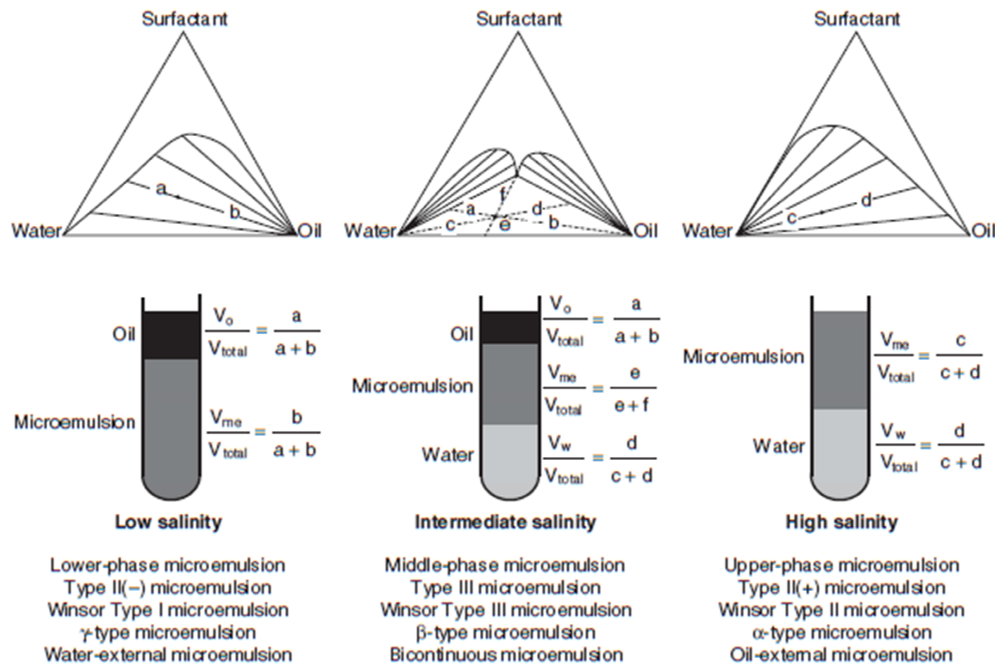


Figure 2-7 – Ternary Diagram for Phase Behavior Experiments with different Salinities (Sheng 2011)

## 2.2.2 Interfacial Tension Measurement

Lowering the IFT is a key objective for EOR since it affects the ultimate recovery. This can be achieved by the use of surfactants. Therefore it is crucial to identify the effect salinity has on surfactants, which decisive for the change in IFT. In the following, two different methods to measure the IFT is explained :

### Pendant Drop Method:

It is an optical method to measure IFT tension and analyze the shape of the pending drop (See Figure 2-8). This can be described using Young-Laplace relation (2.6), which is the balance between gravity, hydrostatic pressure and IFT. The term on the left side of the equation

describes the mean curvature of the droplet,  $\Delta\rho$  is the density difference between the fluids,  $g$  the gravitational acceleration and  $R_0$  the radius of the curvature at position  $y=0$  (See Figure 2-9) (Zeppieri et al. 2001).

$$\left(\frac{1}{R_1} + \frac{1}{R_2}\right) = -\frac{\Delta\rho \times g \times y}{\sigma} + f(R_0) \quad (2.6)$$

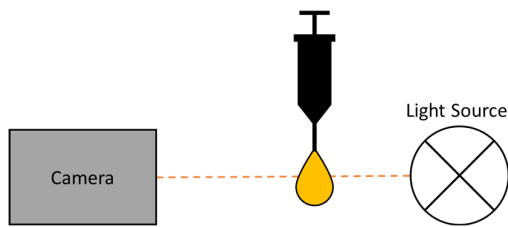


Figure 2-8 – Schematic Sketch of a pendant drop measurement

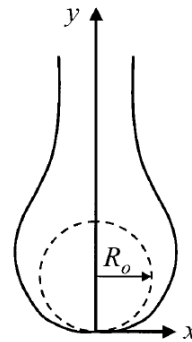


Figure 2-9 – Pendant drop – geometrical variables (Zeppieri et al. 2001)

### Spinning Drop Tensiometer:

A spinning drop tensiometer rotates a liquid, containing a droplet with lesser density, horizontally, forcing the liquid to move towards the capillary wall and causes the droplet to elongate (See Figure 2-10). Interfacial forces hinder the droplet from elongating freely and forcing it to form a spherical shape to reach equilibrium and a stable form. Assuming that the shape can be neglected if the radius is minimal compared to the length following equation can be stated (2.7):

$$\sigma = \frac{\Delta\rho \times \omega^2}{4} R^3 \quad (2.7)$$

Where  $\sigma$  represents the IFT,  $\Delta\rho$  the density difference,  $\omega$  the rotation speed and  $R$  the radius of the droplet. This can then be linked to Young-Laplace and by introducing a shape factor, the IFT can be calculated (Vonnegut 1942).

More detailed information was previously described in (Pit Arnold 2018).

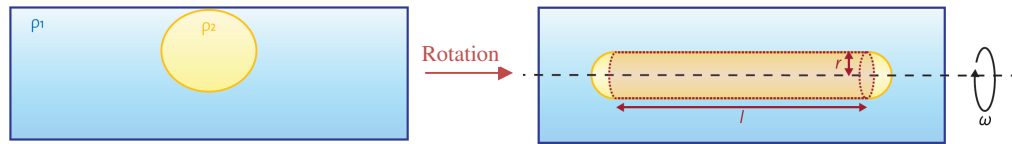


Figure 2-10 – Spinning drop principle (Dataphysics)

### 2.3 Microfluidics in Porous Media

To observe and investigate the behavior of surfactants and the occurring emulsion, microfluidic chips are often used. This part gives a brief overview of selected papers which study the application of microfluidics, surfactants and displacing behavior. More applications can be found in (Gogoi and Gogoi 2019).

Displacement processes through a porous medium are quite complex. Thus, a simplification can lead to many benefits and microfluidic chips provide such a feature. Some of those benefits are the reduced liquid volume, relatively fast experiments, low cost and many more (Zhang et al. 2016). They consist of two plates that are typically fabricated out of a transparent material like glass, silicon-based, or polymer-based materials. Typically, one of these plates has a structure edged or molded into it, presenting an artificial rock structure (Hsu et al. 2017) or a more functional structure like a droplet maker.

For a long time, silicon had been the primary material for microfluidic chip manufacturing. However, this holds some disadvantages like price and opaqueness of the silicone. Therefore, other materials had been utilized like glass and polymer-based substances, as well as geomaterial. Silicon, glass and polymer-based microfluidic chips can either be fabricated using photolithography or soft lithography. Photolithography required many steps to create a microfluidic pattern and is therefore quite expensive. On the other hand, the soft lithography method is inexpensive and easy to reproduce since a master mold can be created and reused. Geomaterial chips are laser-etched rock substrates that hold the advantage that the fluid-rock interactions can be investigated, which are essential mechanisms for the oil and gas industry (Gerami et al. 2019).

Microfluidic chips can be coated in a way that they are either hydrophobic or hydrophilic. Kole and Bikkina investigated the effects of those wettabilities on surfactants by utilizing a hydrophobic and hydrophilic droplet-generation chip (Kole and Bikkina 2017). Additionally,

they also analyzed how different salt types and concentrations impact the emulsion. They injected n-hexadecane, n-decane and a mixture of Span-80 and n-decane as the oleic phase and deionized water, brine solutions (NaCl, KCl, CaCl<sub>2</sub>) and sodium dodecyl sulfate solutions as aqueous phases. They found that the salt type and concentration have a mitigating effect on the droplet diameter of the emulsions. At the same time, surfactants lead to a sharp diameter decline till the CMC is reached, followed by almost no change. Also, increasing the flow rate of the continuous phase leads to a decrease in droplet diameter, while the change in flow rate for the droplet phase showed no effect. An influence of the wettability of the microfluidic chip could be observed and affected the droplet size as well. The hydrophilic chip showed much larger droplets (25 – 30  $\mu\text{m}$ ) compared to the hydrophobic chip (Kole and Bikkina 2017).

Later, Liu investigated the droplet size and distribution of emulsions using different geometric designs, like micro-channel array, T-junction, flow focusing, co-flowing and membrane systems (Liu et al. 2020). They found that the droplet breakup is the result of interfacial, viscous and inertial forces competing with each other and can generally be split into spontaneous transformation, pressure-/flow-driven, shear driven, or Rayleigh capillary instability (interface instability between two fluids). In Figure 2-11 we can see a T-junction chip with different cross-flow configurations. For the squeezing regime, the flow rate of the continuous phase is low; therefore, the dispersed phase fills up the inflow channel until it is blocked. The continuous phase then squeezes the neck of the disperse phase until it detaches. Exceeding a certain capillary number (value depends on channel size, flow rate ratio and viscosity ratio) leads to a dripping regime, where shear stresses cause the necking. For jetting regimes, both flow rates have to be increased, so they flow parallel. They found that the design highly influences the droplet formation. However, keeping the geometry consistent, viscosity and flow rates are the main influence.

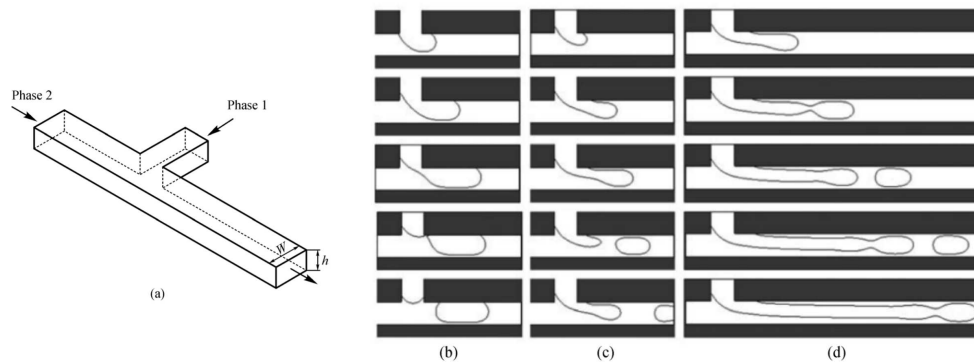


Figure 2-11 – T-junction with different flow regimes: geometry (a), squeezing regime (b), dripping regime (c), jetting regime (d) (Liu et al. 2020)

While the previous papers focused on general emulsion formation, Broens investigated the impact of dead-end pores on the formation of emulsion (Broens and Unsal 2018). In Figure 2-12 three of their performed experiments can be seen, as well as the general structure of the dead-end pore. Focusing on experiment #2, we can see that the pure oil phase is represented in yellow, the emulsion in yellow and the exit point is labeled with "A". At A, we can also find the lowest pressure point, due to the flow direction, making it the best place for the displaced fluid to escape. After 2.5 hours, the emulsion propagated further into the channel and mobilized additional oil. Interestingly, at the end of the dead-pore channel, it can be observed that the emulsion moved along the edges of the channel and filled the corners.

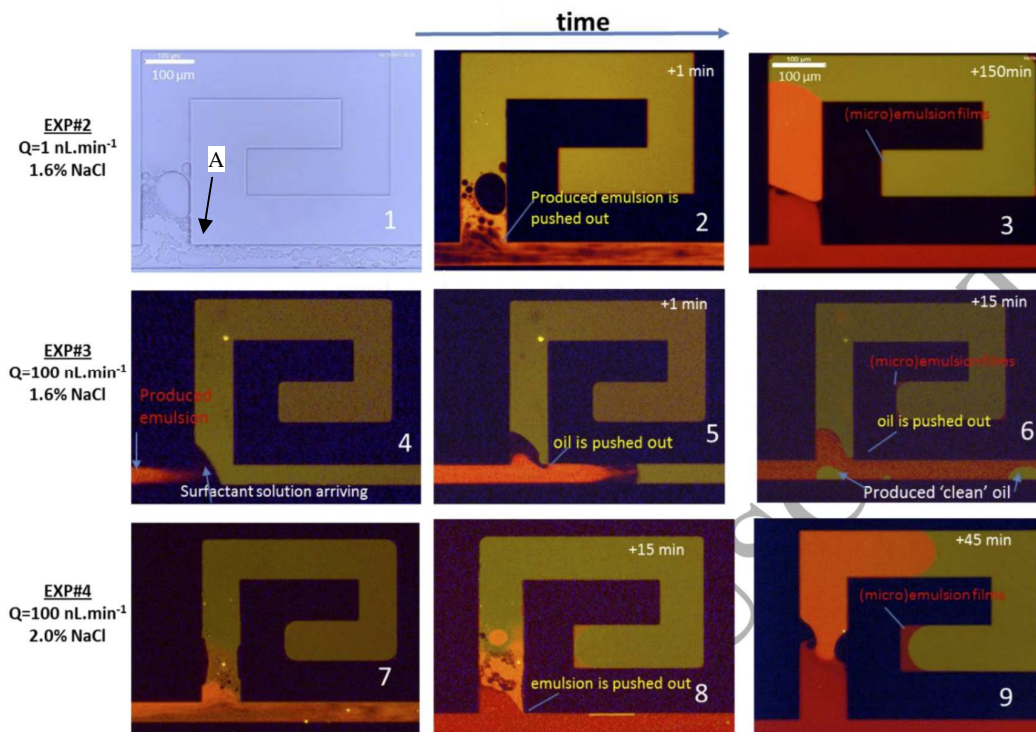


Figure 2-12 – Emulsion formation for an *n*-decane filled dead-end pore for under-optimum and over-optimum salinities and varying injection rates (Broens and Unsal 2018)

Their findings state that the rate at which the aqueous solution, containing the surfactant, was provided to the dead-end pore, affects the formation of emulsion, which is improved with increasing injection rate. The extension length controls the emulsion penetration depth. Extension far away from the main flow channel, even though emulsions are formed, the driving force was not sufficient enough to produce oil. On the other hand, the shallower the extension, the better the recovery.



# Chapter 3

## Experimental Utensils

This chapter discusses all the apparatus, chemicals and programs used in this thesis to perform the experiments and analyze them.

### 3.1 Apparatus

Throughout this thesis, three different kinds of experiments were performed: microfluidic experiments, IFT tension measurements and phase behaviors. For the microfluidic setting, a microscope (3.1.1), a syringe pump (3.1.3) and a micromodel (3.1.2) were used. The IFT tension measurements were performed with a spinning drop tensiometer (3.1.6) and a contact angle measurement and contour analysis system (3.1.5). Phase behaviors required a tube rotator (3.1.4).

#### 3.1.1 Microscope

The microfluidic experiments were captured with a Leica DMi 8 inverted light microscope with five objectives that allow for a magnification of 2.5x, 5x, 10x, 20x and 50x. In this thesis, only 2.5x and 5x magnifications were used. It also offers different types of incident light illumination (ILL) with the possibility of fluorescence lighting. Images are taken with a Leica DMC2900 camera with a pixel size of 1.8 $\mu$ m. The microscope and camera can be controlled by the Leica Application Suite (LAS), which offers an automatic stitching mode to show the whole domain.

#### 3.1.2 Micromodel & Chip holder

Flooding experiments were performed using a chip with a rock pattern out of borosilicate glass from the company Micronit which was placed into a chip holder. These chips come in three different patterns: physical rock network (See Figure 3-1), random network and uniform

network. The physical rock network is based on rock cuttings randomly put next to each other to resemble a pore and throat network. and Even though simulations based on data achieved from this pattern are harder to perform (Micronit), it was more important for this thesis to analyze the behavior obtaining the best connection to real life.

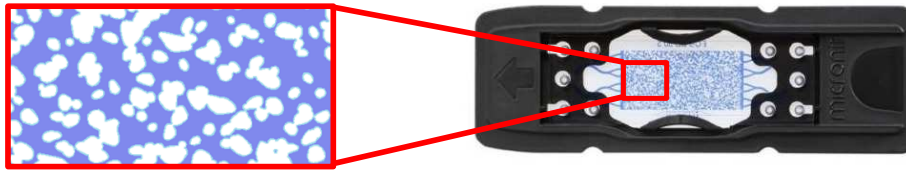


Figure 3-1 – EOR Physical Rock Network – Microfluidic Chip (Micronit)

Table 1 – Dimensions of Physical Rock Network - Microfluidic Chip (Micronit)

Channel height	20 $\mu\text{m}$
Chip thickness	1800 $\mu\text{m}$
Porous domain	2 x 1 cm
Chip material	Borosilicate glass
Number of inlets	1
Number of outlets	1
Permeability	2.5 Darcy
Porosity	0.57
Rockpore volume	2.3 $\mu\text{l}$

### 3.1.3 Syringe Pump

The Chemyx Fusion 200 was used for the injection during all experiments. It allows for a precise infusion with different syringes utilizing a stepper motor, while displaying the rate and injected volume (Chmeyx 2020). Two different syringes were used, a Hamilton Glass Syringe (Diameter: 14.67 mm; Volume: 10 ml) for the injection of oil and a BD plastic syringe (Diameter: 15.9 mm; Volume: 10 ml) for all other liquids.

### 3.1.4 Tube rotator & Phase behavior

To ensure that the mixing force of the phase behavior experiments is done equally, a Multi-Purpose Tube Rotator from Fisherbrand was used. It allows the mounting of 15 phase behaviors simultaneously and a rotating speed ranging from 5 to 80 rounds per minute (Fisher Scientific).

The phase behaviors were done in 15ml centrifugal glasses from the company Carl Roth.

### 3.1.5 Pendant Drop

A contact angle measuring and contour analysis system – OCA 100 from the company Dataphysics was used to perform the pendant drop measurements. It has a measuring range for the IFT tension from  $1 \times 10^{-3}$  to  $2 \times 10^3$  mN/m and a minimum resolution of  $\pm 0.001$  mN/m. The camera has a maximum resolution of 2048 x 1088 pixels and the glass cell (dimension: 40 x 40 x 40 mm) is illuminated by an adjustable LED unit. The droplet was dispensed by a dosing needle (SNC 165/119 Dataphysics) and captured automatically by the included software on a computer (Dataphysics).

### 3.1.6 Spinning Drop Tensiometer

Additional IFT tension measurements were executed with the SVT 20N from Dataphysics. It allows for a temperature control ranging from -10 to 130°C, a rotational speed up to 20 000 revolutions per minute and an IFT tension measuring device of  $1 \times 10^{-6}$  to  $2 \times 10^3$  mN/m. A fast exchange capillary (FEC 622/400-HT Dataphysics) was used with it. It includes a septum which allows for droplet injection while the capillary is rotating (Dataphysics).

## 3.2 Chemicals

Table 2 gives an overview of all the chemicals used during the experiments and are described in more detail below.

Table 2 – Chemicals

Name	Brand	Purpose	Density
Ernodett - J13131	Shell	Surfactant	$\sim 1$ g/cm <sup>3</sup>
2-Butanol - 96870	Sigma-Aldrich	Co-Surfactant	0.81 g/cm <sup>3</sup>
Sodium Chloride - 3957	Carl Roth	Salt	2.17 g/cm <sup>3</sup>
Double distilled Water	Carl Roth	Solution Base	1.0 g/cm <sup>3</sup>
n-Decane 99% - 3475.3	Carl Roth	Oil Phase	0.73 g/cm <sup>3</sup>
Sudan II	Carl Roth	Oil Coloring Agent	-
Fluorescein sodium salt – F6377	Sigma-Aldrich	Fluorescent Tracer	-
Acetone	Sigma-Aldrich	Cleaning	-

#### Surfactant:

The surfactant used in this thesis is alcohol alkoxy sulfate with a maximum application temperature of up to 80°C and an optimum salinity range (NaCl) from 0.5 to 2%, according to the manual (Shell Chemicals).

**2-Butanol:**

To improve the aqueous solubility and to reduce the microemulsion viscosity, 2-Butanol as a cosolvent is added.

**Sudan II:**

Since the surfactant solution and decane are clear liquids and thus hard to distinguish, a fat-soluble dye (Sudan II) is added to the decane, which gives the oleic phase a red to orange color.

**Fluorescein Sodium salt:**

For further visibility enhancement of the emulsion, a fluorescent xanthene dye was added to the aqueous solution. The orange to brown looking powder has an excitation wavelength of 460 nm and an emission wavelength of 515 nm, with a solubility in water of 1 mg/ml.

## 3.3 Programs

The main program used to analyze the images in this thesis was ImageJ and.

### 3.3.1 Image J

ImageJ is an open-source program based on Java, which allows image editing, enhancing and analyzing. Since it is open-source software, many plugins are available. One plugin used during this thesis is the versatile wand tool (ImageJ) which allows the selection of areas with the same or similar (within a tolerance) color or gray value.

## Chapter 4

### Experimental Setup, Methodology & Analysis

The following part gives insight into the performed experiments and their analysis, based on the devices explained in Chapter 3.

#### 4.1 Microfluidic Displacement

##### 4.1.1 Injected Solutions

The solutions were measured using a highly precise scale (Kern ABJ320-4NM) with a minimum weight of 1mg, which was especially important for measuring the fluorescein sodium salt. During the fluorescence intensity analysis (See 5.1.1), it was observed that 100mg of fluorescein sodium salt per one liter solution result in optimum visibility. During phase behavior experiments (See 5.2.3), it was confirmed that the tracer does not influence the result and it is assumed that this also holds for dynamic experiments.

Three different solutions were mixed with varying salinity (Table 3). The amount of co-surfactant and surfactant stayed the same for all solutions. Therefore, only the base solutions (NaCl and DI-W) were adjusted. The salinity ranged from 1%, 2% and 4%, where the percentage refers to weight-volume-percentage. A salinity of 1% equals 1 gram or 0.462ml of NaCl and 99.538ml of DI-W.

*Table 3 – Solution for Fluorescent Displacement Experiments*

#	Salinity	NaCl [g]	DI-W [g]	2-Butanol [g]	J13131 [g]	Fl-salt
1.1	1%	1 g	99.538 g	2 g	0.5 g	100 mg/l
1.2	2%	2 g	99.078 g			
1.3	4%	4 g	98.157 g			

### 4.1.2 Setup

Figure 4-1 shows the experimental setup for the fluorescent displacement experiments with the syringe pump (1), syringe (2), inlet valve (3), inlet (4), outlet (5), micromodel (6), outlet valve (7), waste tank (8) and microscope (9).

It was essential to ensure that the length and position of the connection cables were not changed for the experiment since it influences the timing, the pressure and the fluid distribution.



Figure 4-1 – Experimental Setup – Microfluidic Displacement

### 4.1.3 Cleaning & Injection

To assure consistent starting conditions for all microfluidic experiments, the chip was cleaned in the following order:

- Injection of 3 ml water to displace the aqueous solution
- Injection of 2ml acetone to displace oil
- Injection of air till no acetone is evaporated

Vacuum with closed inlet valve for approximately 3 hours. Then the chip was saturated with 99.9% n-decane plus Sudan II first with a high injection rate to displace the air in the tube and then for at least one hour with an injection rate of 0.00193 ml/h. The inlet valve was then closed and a syringe with the aqueous solution was connected. Once the solution passed through the inlet pipe, the injection rate was set to 0.00193 ml/h. After 15 minutes, the inlet valve was opened and the image capturing was started. Figure 4-2 demonstrates the segmented image of the used micromodel in this study. The grains are indicated by black color where the fluid pathway (pores) are silver. Please note that the injection direction was from left to right

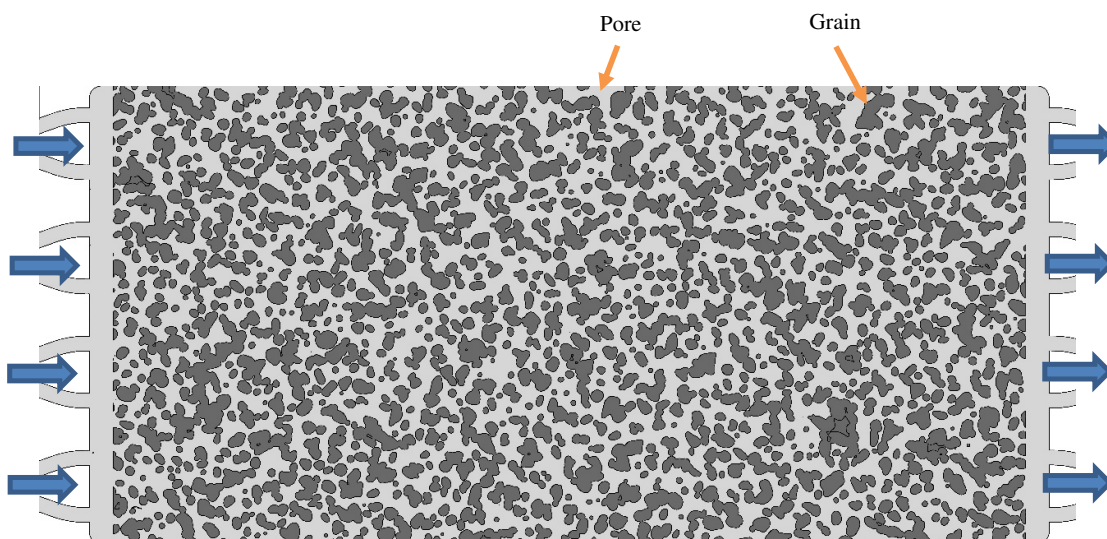


Figure 4-2 – Closeup of micromodel structure with injection direction from left to right

#### 4.1.4 Fluorescent Image Capturing

For the fluorescent Image Capturing, the ILL was set to fluorescent in the program LAS X and the micromodel was covered to blackout all external lighting. The exposure time was set to 2 ms and a magnification of 2.5x (field of view: 3742 x 2806 $\mu\text{m}$ ) was chosen (See Figure 4-3).



Figure 4-3 – Settings for fluorescent image capturing in LAS X

After the fluid was injected, a time interval with tile scan was started, covering the whole domain. The entire image was split into 7 x 5, resulting in a total number of 35 stages. The positions of those were kept the same for all experiments to make them comparable. The timed interval was not set in a specific order, but all final images were taken after fluid motion could not be observed anymore.

#### 4.1.5 Fluorescent Intensity Analysis

An intensity analysis was performed to analyze the final data and to find the best amount of fluorescent sodium salt for enhanced emulsion visibility. To do so, eight different solutions with varying amounts of fluorescent salt were mixed (See Table 4) and were then injected into a micro model. Several tile scans with different magnification and exposure times were taken for each experiment. The best results could be seen with an exposure time of two seconds and a magnification of 2.5.

Table 4 – Solutions for Fluorescent Intensity Analysis

#	Fluorescein salt [mg/l]	Base
2.1	2	Distilled water
2.2	5	Distilled water
2.3	10	Distilled water
2.4	20	Distilled water
2.5	50	Distilled water
2.6	80	Distilled water
2.7	100	Distilled water

2.8	300	Distilled water
-----	-----	-----------------

To identify the fluorescent intensity, the mean grey values (4.1) of the pore space and grains were measured with ImageJ. Since the grains do not emit any fluorescent light, they can be seen as references for the background noise. This background noise has to be removed from the pore mean grey value to get the proper intensity ( $\Delta\text{Mean}$ ) and can be seen in equation (4.2) (Peter Bankhead 2014).

The mean grey value is calculated by dividing the color values on a red, green and blue (RGB) scale by three, to get the average (See equation (4.1)). A value of 255 corresponds to the maximum of either red, green or blue and 0 to the minimum. Hence, white has the code 255/255/255 and black 0/0/0.

$$\text{Mean} = \frac{\text{red} + \text{green} + \text{blue}}{3} \tag{4.1}$$

$$\Delta\text{Mean} = \Delta\text{Mean}_{\text{pore}} - \Delta\text{Mean}_{\text{Grain}} \tag{4.2}$$



Figure 4-4 – RGB color scheme for black (left) and white (right)

The same tile for every experiment was chosen and then a selection mask for the grain and pore area (See Figure 4-5) was created (the selected area is smaller than the actual area). The measurements in ImageJ were set to area and mean gray value (*Analyze > Set Measurements ...*), followed by the actual measurement (*Analyze > Measure*). To calculate the  $\Delta\text{Mean}$ , the results were imported into excel and processed there.

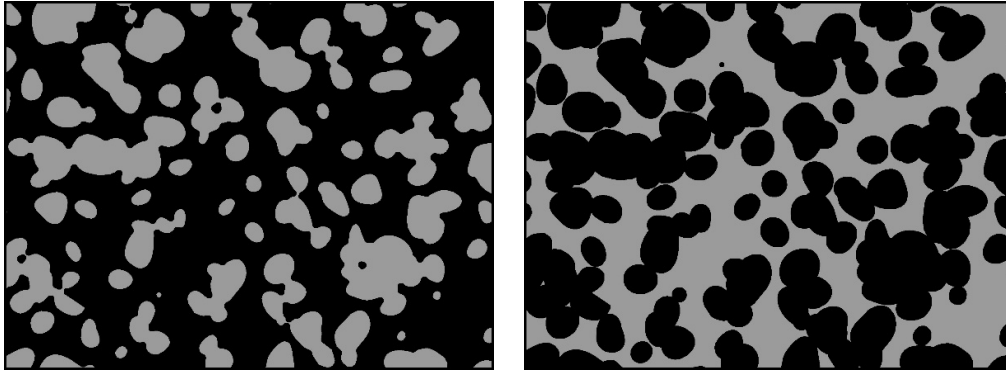


Figure 4-5 – Selection mask for pore (left) and grain area (right)

After the true intensity is calculated, all values can be added into a diagram to find a relationship between fluorescent intensity and fluorescent salt concentration (See Figure 5-3). This relationship can then be used to analyze the percentage of aqueous phase in the fluorescent displacement experiments.

#### 4.1.6 Fluorescent Displacement Analysis

Three different tiles were picked and analyzed for all three experiments at different progression. These images were then analyzed qualitatively by describing observations made, like droplet size, mixing behavior and general displacement.

Additionally, the end stage was analyzed for the fluorescent concentration by applying the findings of the fluorescent intensity analysis. The fluorescein salt concentration of 100 mg/l, which was added to experiment 1.1 – 1.3 (See Table 3), was set as 100% aqueous phase concentration. Thus a value of 0% means a pure oleic phase and values between 0 – 100% indicate a mixture of both.

## 4.2 Characterization of Fluid System

To characterize the fluids, IFT measurements and phase behaviors were performed.

### 4.2.1 Pendant Drop Method

The glass cell was filled with the aqueous solution (See Table 5) then a borosilicate glass plate was placed inside. Then the needle was lowered inside the liquid and placed above the plate. Densities of both the solution and the oil have to be entered into the program, as well as the outer diameter of the dosing needle, which acts as a reference. The dosing needle was then set to dispense at a slow rate, so it could be stopped once a droplet was formed.



Figure 4-6 – Experimental Setup – Pendant Drop

Table 5 – Solutions for Pendant Drop and Spinning Drop Experiments

#	Aqueous Phase	Droplet
3.1	1% NaCl-solution	n-Decane 99.9% + Sudan II
3.2	2% NaCl-solution	n-Decane 99.9% + Sudan II
3.3	4% NaCl-solution	n-Decane 99.9% + Sudan II

#### 4.2.2 Spinning Drop Tensiometer

For the spinning drop tensiometer, the same solutions as for the pendant drop method were used (See Table 5) and were named 4.1 for the 1% NaCl-solution, 4.2 for the 2% NaCl-solution and 4.3 for the 4% NaCl-solution. The temperature control was set to 25°C. The capillary was filled with the aqueous phase, inserted into the rotation chamber. At a slow rotation speed of 300 rpm, the droplet was injected through the septum and the rotation chamber closed off. Then the settings in the program were adjusted (magnification, density, ...) and the speed increased.



Figure 4-7 - - Experimental Setup – Spinning Drop

### 4.2.3 Phase Behavior

The phase behaviors were performed in 15 ml test tubes and sealed with a cork plug. Former experiments revealed that those show the best sealing capability compared to other plugs. Parafilm was then used for additional sealing. The tubes were only filled to the 10ml mark and filled with equal parts of the aqueous solution and oil.

Two groups were created for these experiments. Group 1 (experiment 5.1 – 5.3) were performed with 0.5% surfactant, 2% 2-butanol, 100 mg/l of fluorescein salt and with 1%, 2% or 4% sodium chloride. For group 2 (experiment 6.1 – 6.3) the same solutions were used, however, without the addition of fluorescein salt (See Table 6).

Table 6 – Solutions for Phase Behavior Experiments

#	Aqueous Phase	Oleic Phase
---	---------------	-------------

---

<b>5.1</b>	1% NaCl-solution + Fluorescein salt	5 ml	n-Decane 99.9%	5 ml
<b>5.2</b>	2% NaCl-solution + Fluorescein salt	5 ml	n-Decane 99.9%	5 ml
<b>5.3</b>	4% NaCl-solution + Fluorescein salt	5 ml	n-Decane 99.9%	5 ml
<b>6.1</b>	1% NaCl-solution	5 ml	n-Decane 99.9%	5 ml
<b>6.2</b>	2% NaCl-solution	5 ml	n-Decane 99.9%	5 ml
<b>6.3</b>	4% NaCl-solution	5 ml	n-Decane 99.9%	5 ml

To minimize mixing while preparing the test tubes, they were first filled with 5 ml of aqueous solution followed by 5 ml of decane. They were then put into a tube rotator for 24 hours with a speed of 25 rounds per minute. After the mixing was completed, the tubes were placed vertically in a holder and left to equilibrate at controlled ambient temperature. Photographs of the phase behaviors were taken before and once the phases were separated by gravity at equilibrium conditions.



# Chapter 5

## Results and Discussion

This chapter proposes all results and observations made of the experiments described previously. All experiments are described in Chapter 4 and a complete list can be found in A.1.

In 5.1 the results of all experiments, which were performed using the setup described in 4.1.2, are collected. Starting with the Fluorescent Intensity Analysis and followed by the main experiment Fluorescent Displacement. 4.2 shows the findings of the fluid system characterization, which are intended to support the main experiments.

Phase Behavior experiments and fluorescent intensity analysis were performed first. Fluorescent displacement, pendant drop and spinning tensiometer experiments were done simultaneously.

The purpose of the phase behavior experiments is to show that the fluorescein salt does not affect the surfactant and give an indication about the optimum salinity. In addition, the fluorescent intensity analysis was performed to find the ideal amount of fluorescein salt for the best visibility in the fluorescent displacement analysis and show a relationship between the intensity and the mixing of surfactant solution. To measure the change in IFT, pendant drop and spinning drop experiments were performed. The main experiment, the fluorescent displacement, shows how well the solution distributes, displaces and mixes while being injected.

## 5.1 Microfluidic Displacement

### 5.1.1 Fluorescent Intensity Analysis

Figure 5-1 shows the acquired images for experiments 2.1 to 2.8 (See Table 4) and it can be observed that the concentrations of 2 to 20 mg/l are not visible to the bare eye. This is also supported by the measured results in Table 7 and Table 8, where we can see that the  $\Delta\text{Mean}/\text{Intensity}$  for those concentrations is relatively low, which means that the noise is too great to give a clear statement. Experiment 2.8 with 300 mg/l, however is too bright, which could lead to photo pollution of the grains and therefore distort the results. Therefore, 2.4 (100 mg/l) showed the best compromise from both sides. The solution was visible enough to be distinguished from the grains, but the fluorescein salt was not enough to over glow the grains.

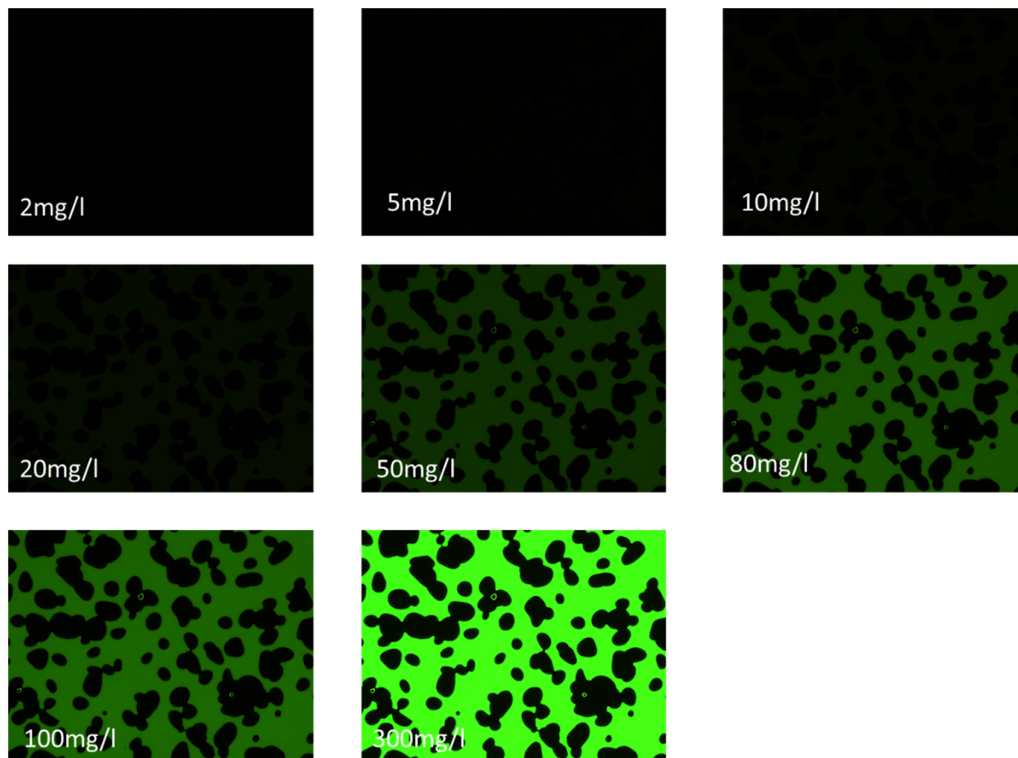


Figure 5-1 – Fluorescent Intensity Analysis Results

Importing the images into ImageJ and analyzing them as described in 4.1.5 showed a linear relationship (See equation (5.1)) between the intensity and the amount of fluorescein salt, which can be seen in Figure 5-2 and Figure 5-3.

Table 7 – Results Fluorescent Intensity Analysis for Experiment 2.1 – 2.4

Experiment	2.1	2.2	2.3	2.4
Fluorescein Salt Concentration [mg/l]	2	5	10	20
Mean <sub>Pore</sub>	0.97	1.67	3.38	6.54
Mean <sub>Grain</sub>	0.52	0.49	0.57	0.75
$\Delta$ Mean	<b>0.45</b>	<b>1.18</b>	<b>3.38</b>	<b>6.54</b>

Table 8 – Results Fluorescent Intensity Analysis for Experiment 2.5 – 2.8

Experiment	2.5	2.6	2.7	2.8
Fluorescein Salt Concentration [mg/l]	50	80	100	300
Mean <sub>Pore</sub>	20.12	33.37	42.76	114.71
Mean <sub>Grain</sub>	1.55	2.42	2.99	8.01
$\Delta$ Mean	<b>18.57</b>	<b>30.95</b>	<b>39.76</b>	<b>106.70</b>

Figure 5-2 shows the  $\Delta$ Mean vs. the fluorescein salt concentration up to 300 mg/l, where a linear trend can be seen. However, since all experiments were performed with 100 mg/l, which equals 100%, Figure 5-3 gives a better statement about the mixing ratio. This relationship can be rewritten seen in (5.2) and was used to calculate the concentration in percent for the fluorescent displacement analysis. Since 100% of aqueous phase is equal to 100 mg/l of fluorescein salt concentration, both terms are interchangeable in this case.

$$\Delta Mean = 39.807 \times \text{Fluorescein Salt Concentration} - 0.6823 \quad (5.1)$$

	$\% \text{ Aqueous Phase} = \frac{\Delta Mean + 0.6823}{39.807}$	(5.2)
--	--	-------

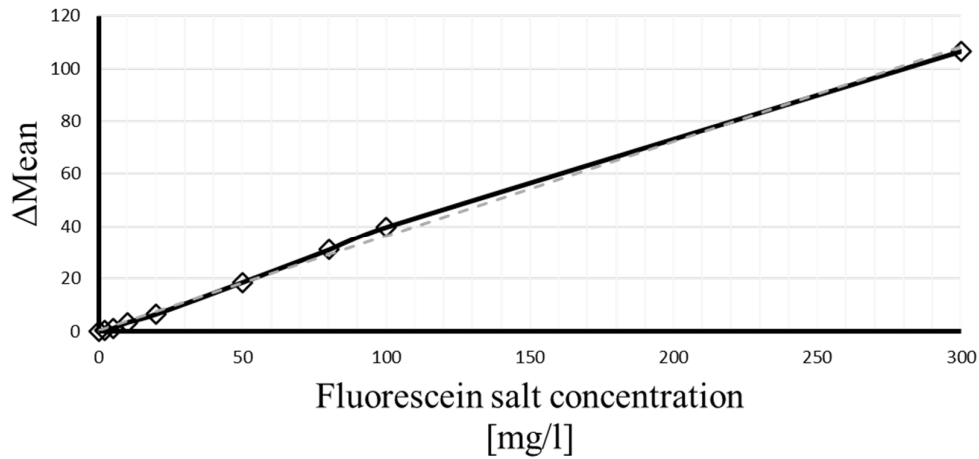


Figure 5-2 – Fluorescent Intensity Analysis:  $\Delta\text{Mean}$  vs. Fluorescein Salt Concentration [mg/l]

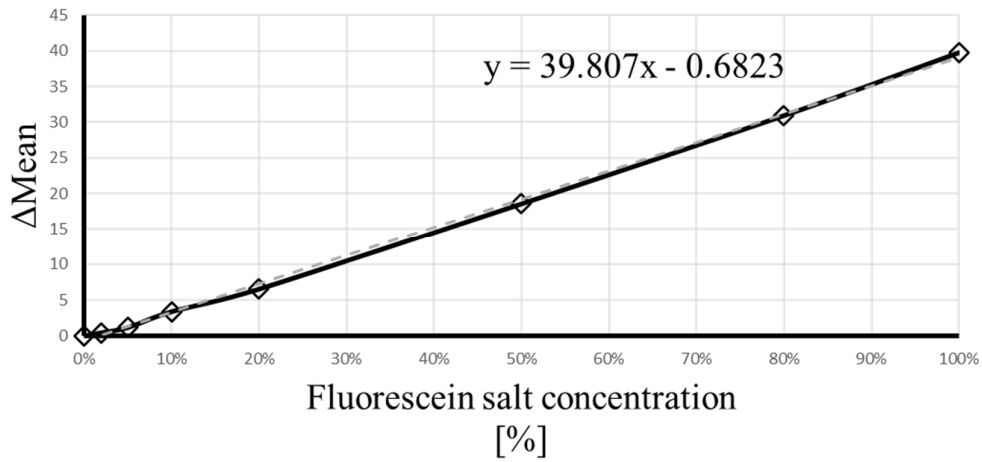


Figure 5-3 – Fluorescent Intensity Analysis:  $\Delta\text{Mean}$  vs. Fluorescein Salt Concentration [%]

Therefore a fluorescein salt concentration in the pore of 100% (100 mg/l fluorescein salt) relates to a pure aqueous phase, while 0% (0 mg/l fluorescein salt) means a pure oleic phase.

### 5.1.2 Fluorescent Displacement Analysis

As described earlier, the image was split into seven times five stages (marked in red) and three of them were chosen to be investigated. Figure 5-4 shows the full domain and the position of the selected stages and Figure 5-5 displays the stages up close. Stage 06 is close to the inlet and contains a dead-end pore open against flow direction, which means that the fluid contained in it is harder to displace since it has no way to escape. Stage 12 is neither close to the inlet nor the outlet and has open pores easy to access. Stage 28 is close to the outlet and contains a dead-end pore in flow direction and perpendicular to it. Additional to the fluorescent image capturing, one image without fluorescent ILL was taken to visualize the position of the oil and grains. Applying the findings of the fluorescence intensity analysis, the endstages were evaluated for aqueous phase content and emulsions. Furthermore, the fully merged image in the end state, where no change could be observed anymore, was analyzed.

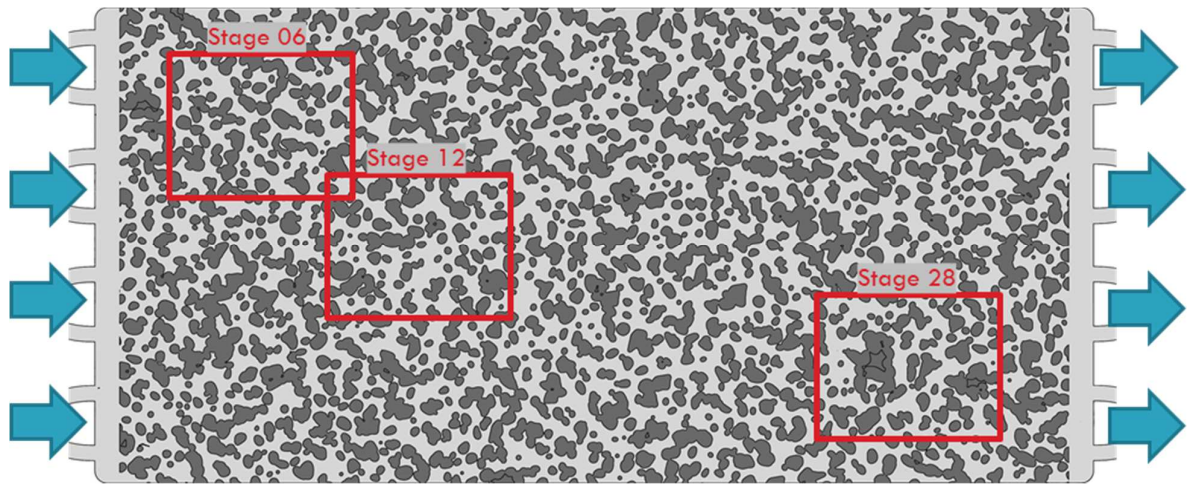


Figure 5-4 – Micromodel with labeled stages (red)

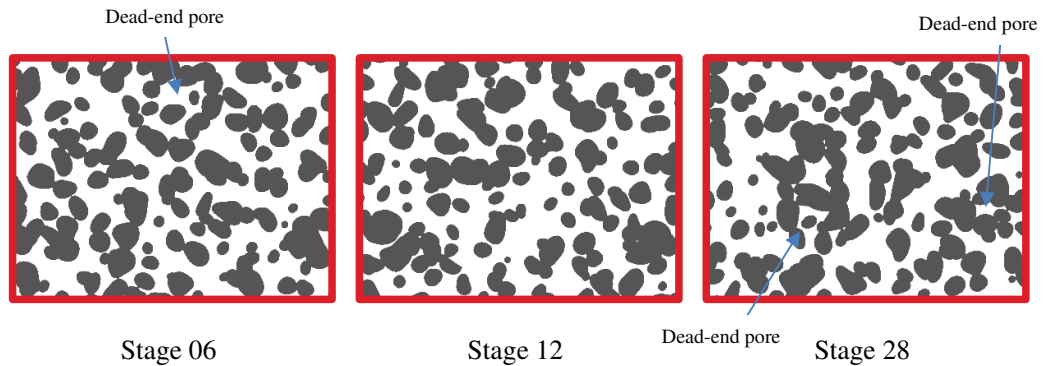


Figure 5-5 – Selected Stages

### 5.1.2.1 Stage 06

Observing Figure 5-6 (experiment 1.1) it can be seen that the solution emerges from above and not in flow direction, which indicates that at first a larger area must have been bypassed. Also, the dead-end pore stays untouched and mixing of the fluid happens only in the early times. The scale bar in the upper right picture is valid for all following stage images (Figure 5-6 - Figure 5-22).

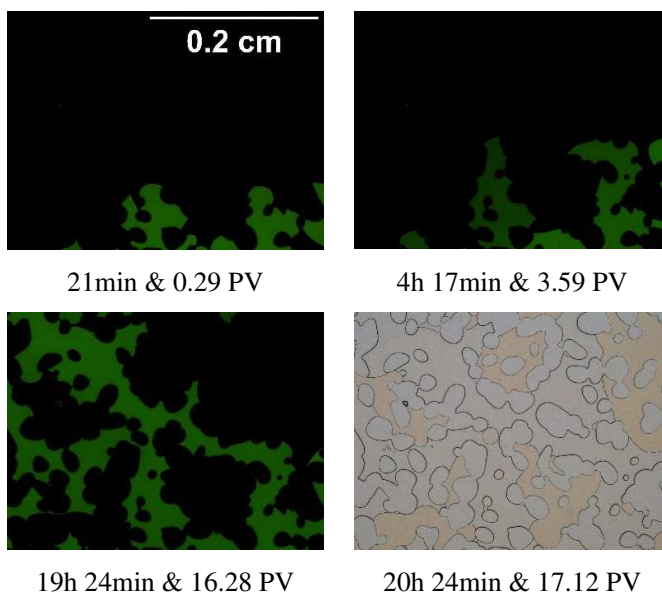
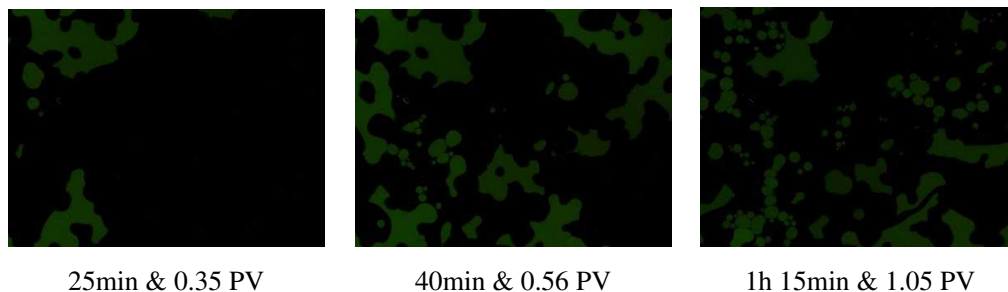


Figure 5-6 – Experiment 1.1 (1% NaCl) – Stage 06

For experiment 1.2 (See Figure 5-7), a more uniform fluid distribution can be seen. Small separated clusters are initially formed. And as time progresses, they start to connect. Looking at the intensity, we can say that those clusters are mixtures of the oleic and aqueous phase and therefore emulsions. A wide variety of mixing ratios can be observed during the experiment, which appear to form clusters depending on the fluorescent salt concentration. At the end state, these clusters are not as prominent anymore but are still visible.



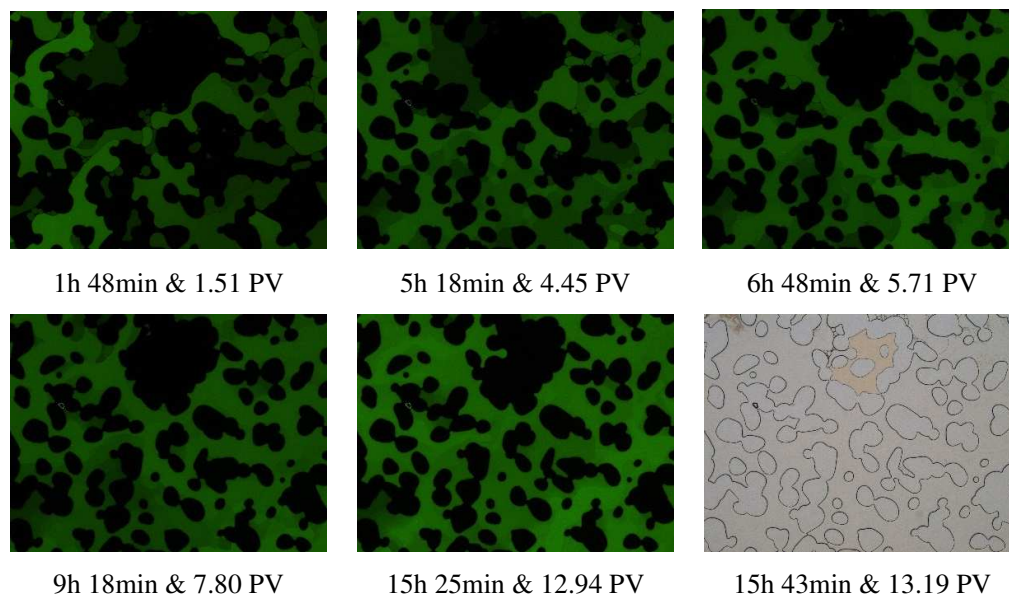


Figure 5-7 – Experiment 1.2 (2% NaCl) – Stage 06

For the 4% NaCl solution (See Figure 5-8), the clusters with varying fluorescent salt concentrations stayed intact even at the end of the experiment. This becomes even more obvious looking at the image taken without fluorescent ILL (lower right corner). Due to light refraction, some areas appear to be brown since they contain a large amount of very small droplets, which could be seen as emulsions.

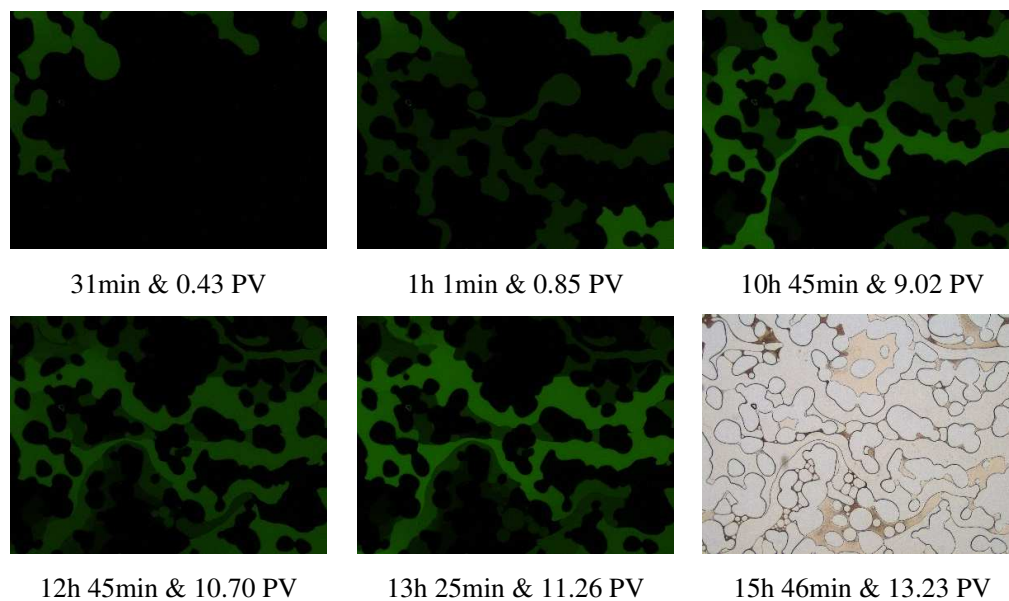


Figure 5-8 – Experiment 1.3 (4% NaCl) – Stage 06

None of the solutions penetrated the dead-end pore fully, whereby experiment 1.2 penetrated it the furthest and seemed to have the best displacement overall compared to the other solutions.

### 5.1.2.2 Stage 12

For Stage 12, experiment 1.2 only showed significant changes at the beginning of the experiment regarding the mixing and distribution. Small oil clusters can be seen in between the grains, which do not seem to be attached to the grains and therefore could easily be transported.

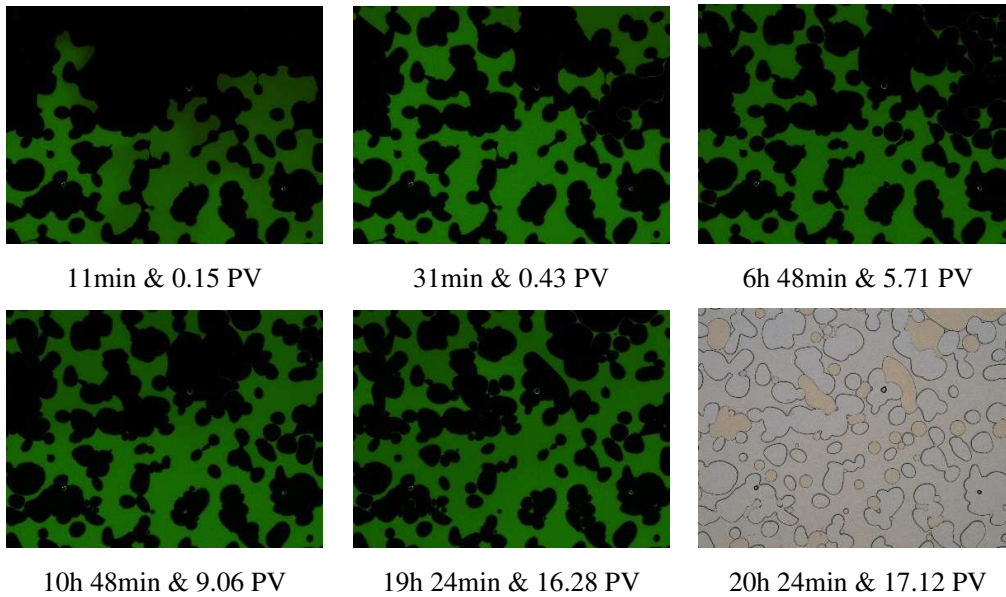
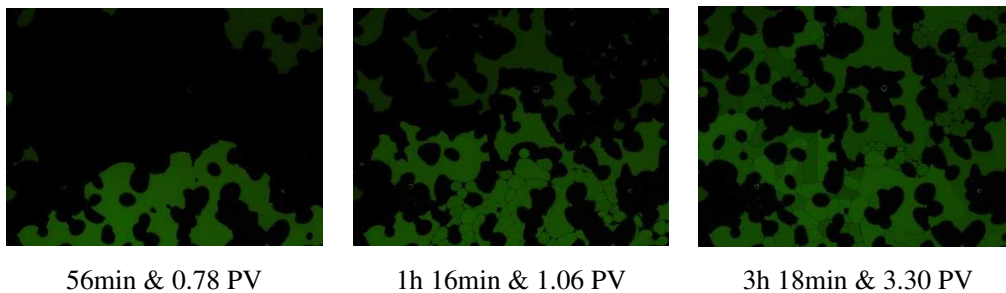


Figure 5-9 – Experiment 1.1 (1% NaCl) – Stage 12

No visible oil was left at the end in Figure 5-10. Only the tiny color variation indicates that some oil must be mixed within the solution. At 1 hour and 16 minutes, after entering the micromodel, clusters are formed, which do have a small film of oil in between them. Over time, the film becomes thinner, till it disappears, which means that the oil solubilized due to a decrease in IFT.



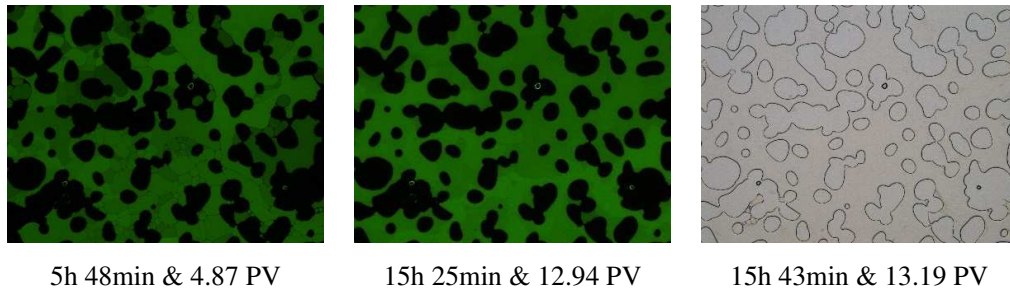


Figure 5-10 – Experiment 1.2 (2% NaCl) – Stage 12

On the other hand, a clear boundary stayed consistent till the end of experiment 1.3 (See Figure 5-11). While the intensity of the color was quite intense for the upper and lower part of Stage 12, the middle tended to mix not as strong with the oil.

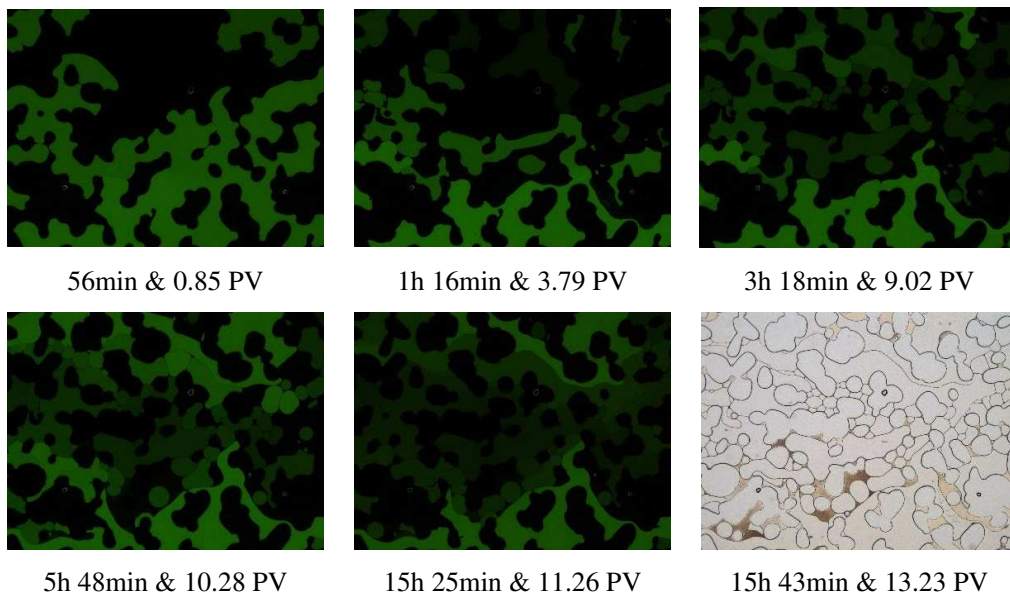
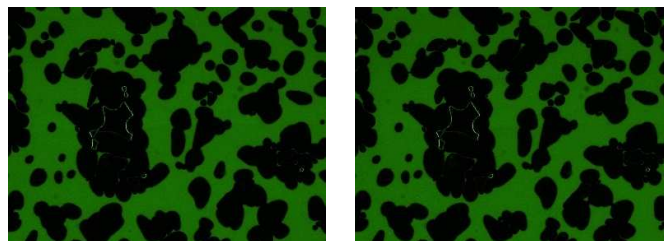


Figure 5-11 – Experiment 1.3 (4% NaCl) – Stage 12

### 5.1.2.3 Stage 28

For Stage 28, where two types of dead-end pores are present, we can see for experiment 1.1 that neither of them got flooded. We can observe the same behavior as for Stage 12 of the separated oil clusters and that the fluid distribution stayed consistent over time.



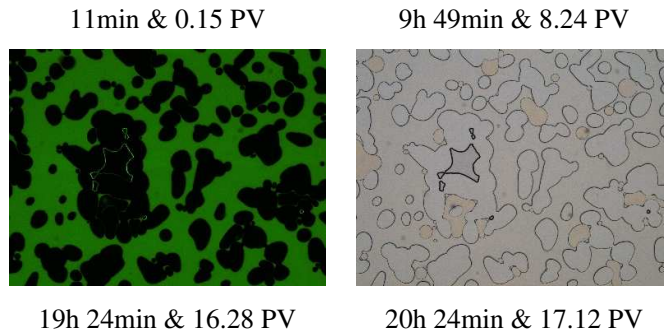


Figure 5-12 – Experiment 1.1 (1% NaCl) – Stage 28

For experiment 1.2, however, we can see the formation of small droplets with decreasing size over time. At the end stage, the borders between the clusters seem to disappear and only intensity variations indicate something different. However, the image without fluorescent ILL, shows that the droplet size decreased even further. Both dead-end pores got invaded, still with some residual oil inside.

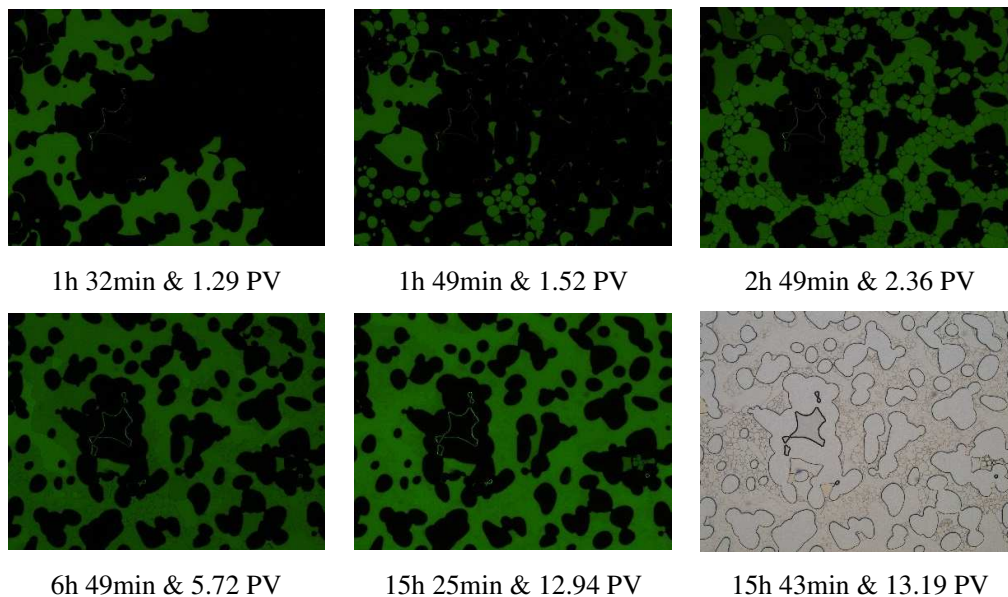


Figure 5-13 – Experiment 1.2 (2% NaCl) – Stage 28

Interestingly, we can see in Figure 5-14 that the dead-end pore is covered with a thin film of aqueous solution, which provides a pathway for coming solution, filling up the end of the pore and pushing the oil out.

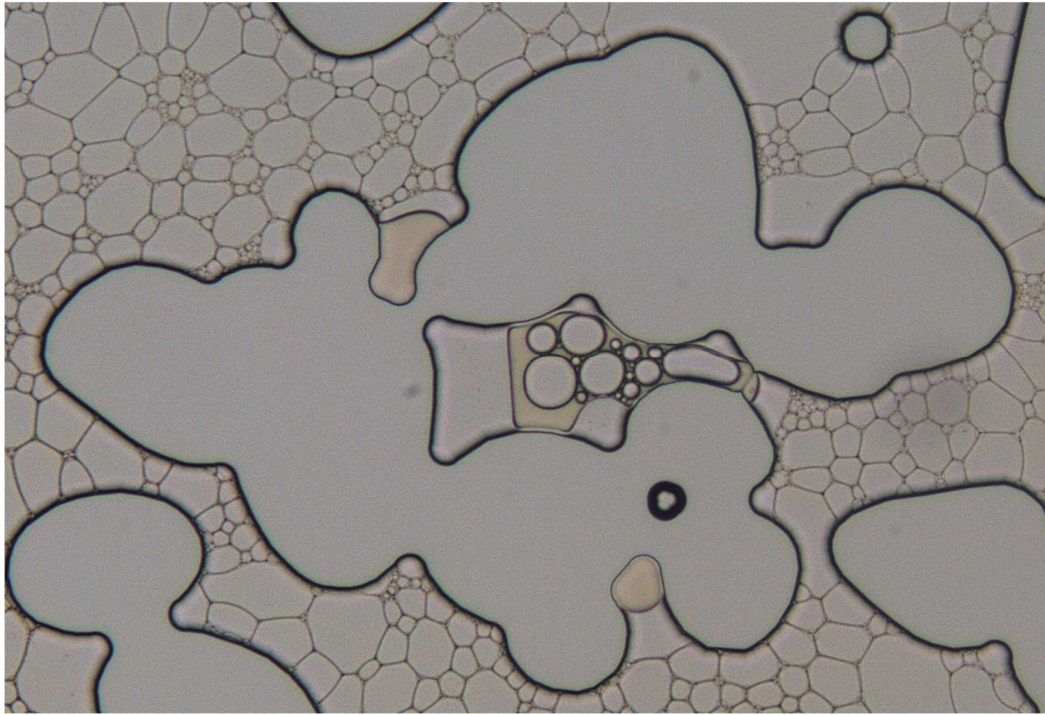


Figure 5-14 – Experiment 1.2 (2% NaCl) – Stage 28 Zoom In – dead-end pore

In Figure 5-15, none of those pores got penetrated by the 4% NaCl-solution and a considerable amount of oil was bypassed.

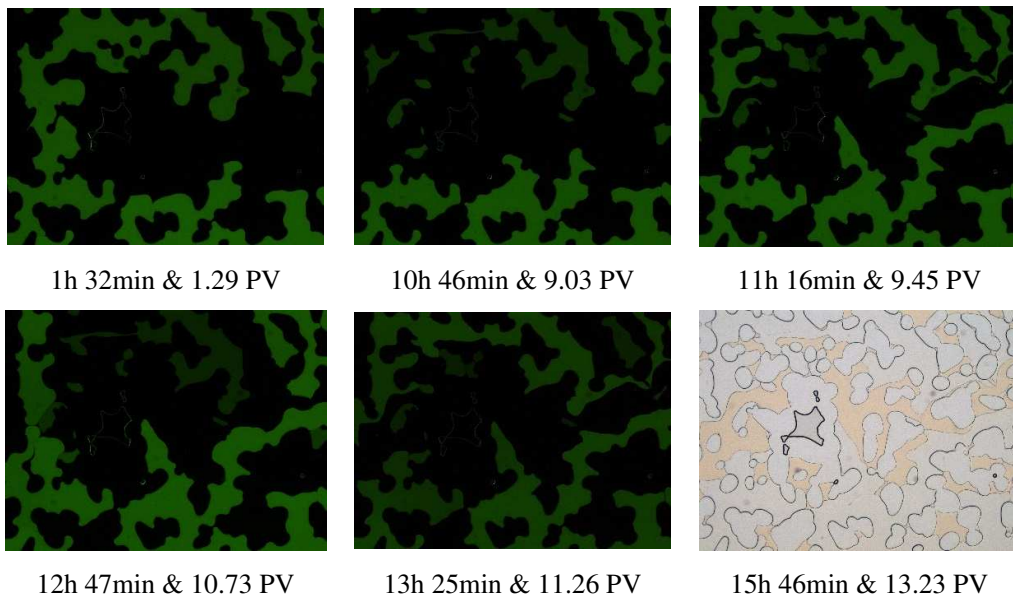


Figure 5-15 – Experiment 1.3 (4% NaCl) – Stage 28

In general it can be stated that only experiment 1.2 invaded both dead-end pores, while 1.1 left some small oil droplets and 1.3 even bypassed large areas of oil.



### 5.1.2.4 Mixing Analysis

In this part, the final images are analyzed for their mixing behavior by measuring the  $\Delta$ Mean and applying the relationship found in 5.1.1. Images shown here are enhanced in brightness and contrast, however, all measurements were performed on the original images. Since experiment 1.1 showed an average of aqueous phase concentration between 80 and 90 %, it is not described here but can be found in A.2. As can be seen in the following images, values over 100% appear, which would state that the amount of water exceeds 100%. Since the percentage of the aqueous solution equals the amount of fluorescein salt, one reason could be that the salt aggregates and excess exists at this location. Another reason could be the deviation of the trendline or environmental changes (light for example) during image capturing.

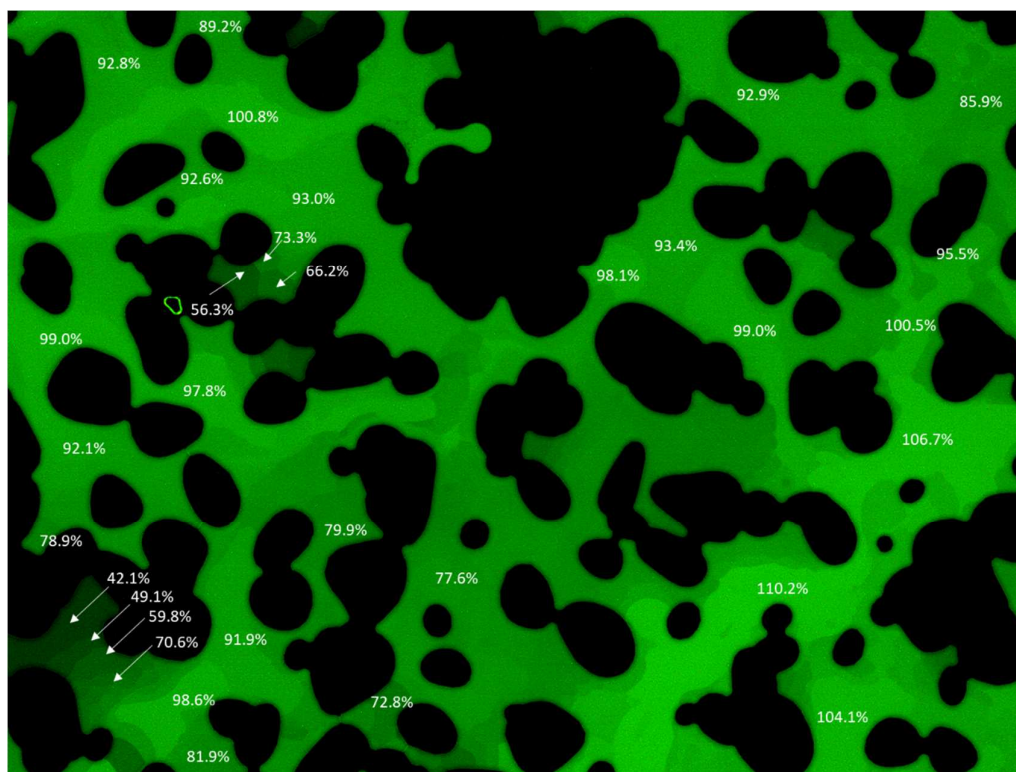


Figure 5-16 – Experiment 1.2 (2% NaCl) – Stage 06 – Mixing Analysis

In the lower-left corner of Figure 5-16 a mixing gradient can be observed starting from 42% of aqueous solution, which enhances the further away we get from this pore. This means that areas that are enclosed are harder to reach. While Figure 5-17 shows an overall more even distribution, we can observe in Figure 5-18 and Figure 5-19 smaller droplets which do not coalesce.

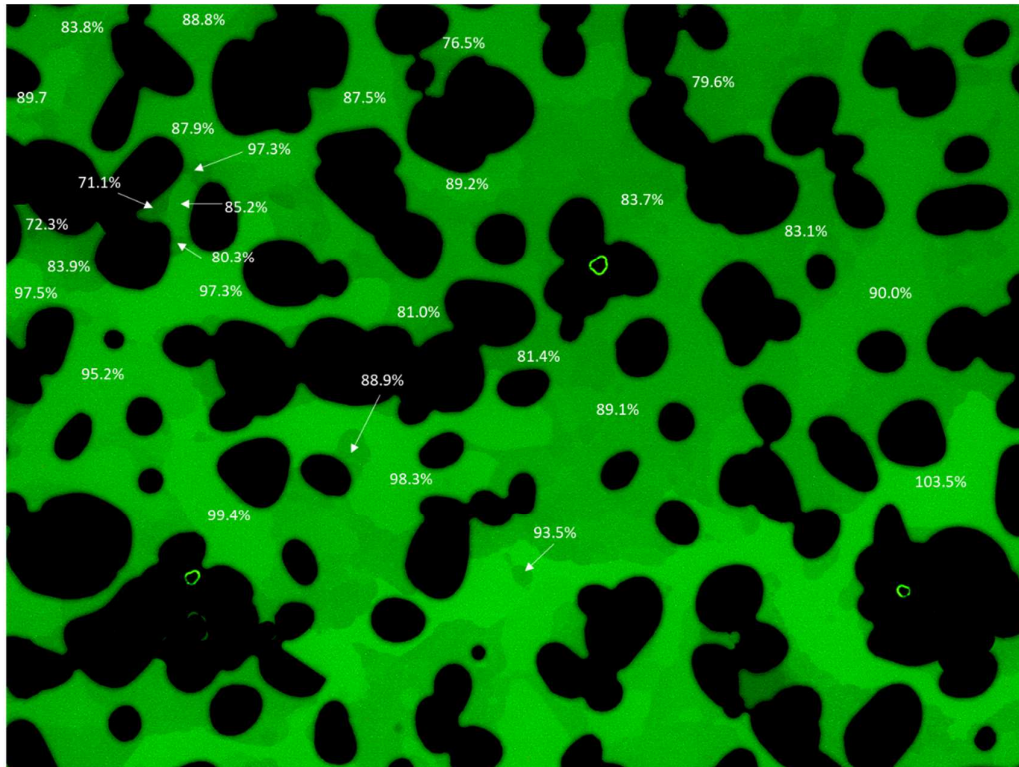


Figure 5-17 – Experiment 1.2 (2% NaCl) – Stage 12 – Mixing Analysis

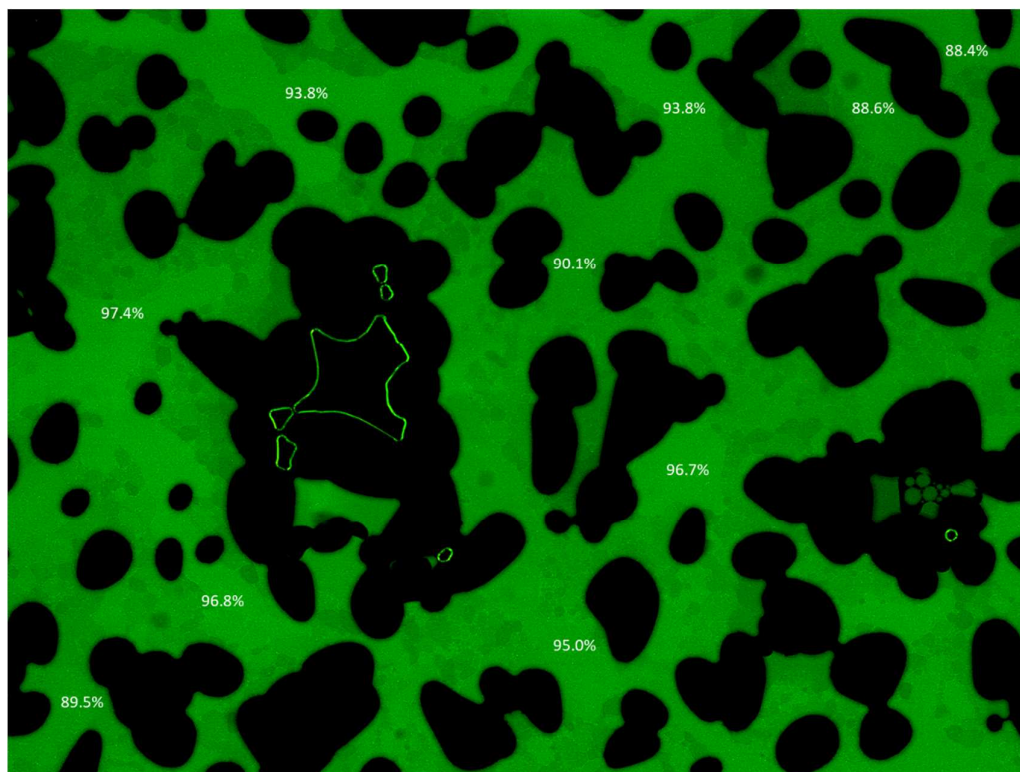


Figure 5-18 – Experiment 1.2 (2% NaCl) – Stage 28 – Mixing Analysis

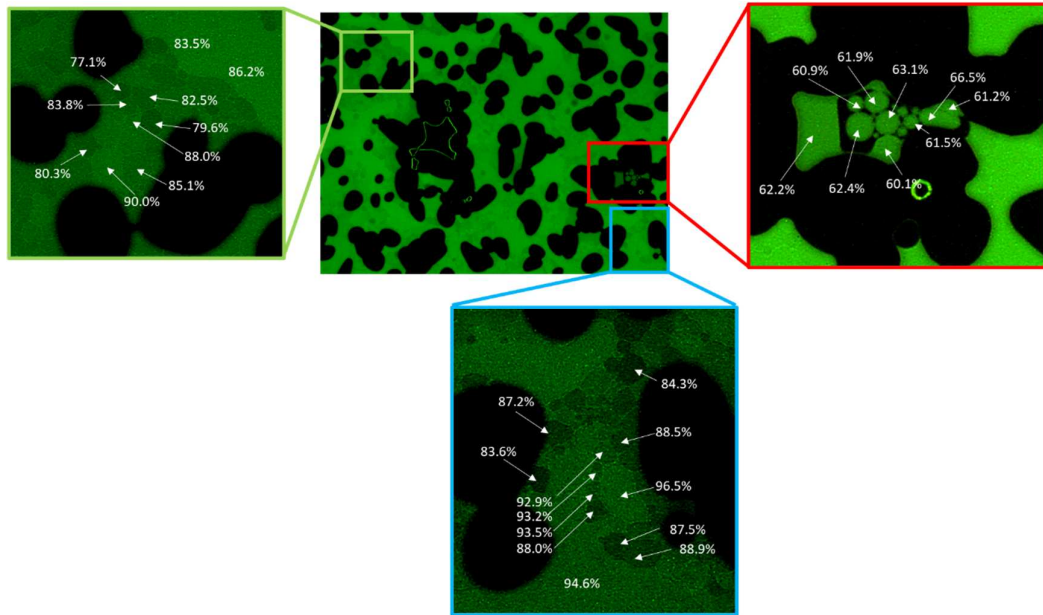


Figure 5-19 – Experiment 1.2 (2% NaCl) – Stage 28 Zoom in – Mixing analysis

Figure 5-20, Figure 5-21 and Figure 5-22 show a wide variation of mixing behavior and an obvious flow path can be observed where the aqueous phase is most present and clear borders can be seen.

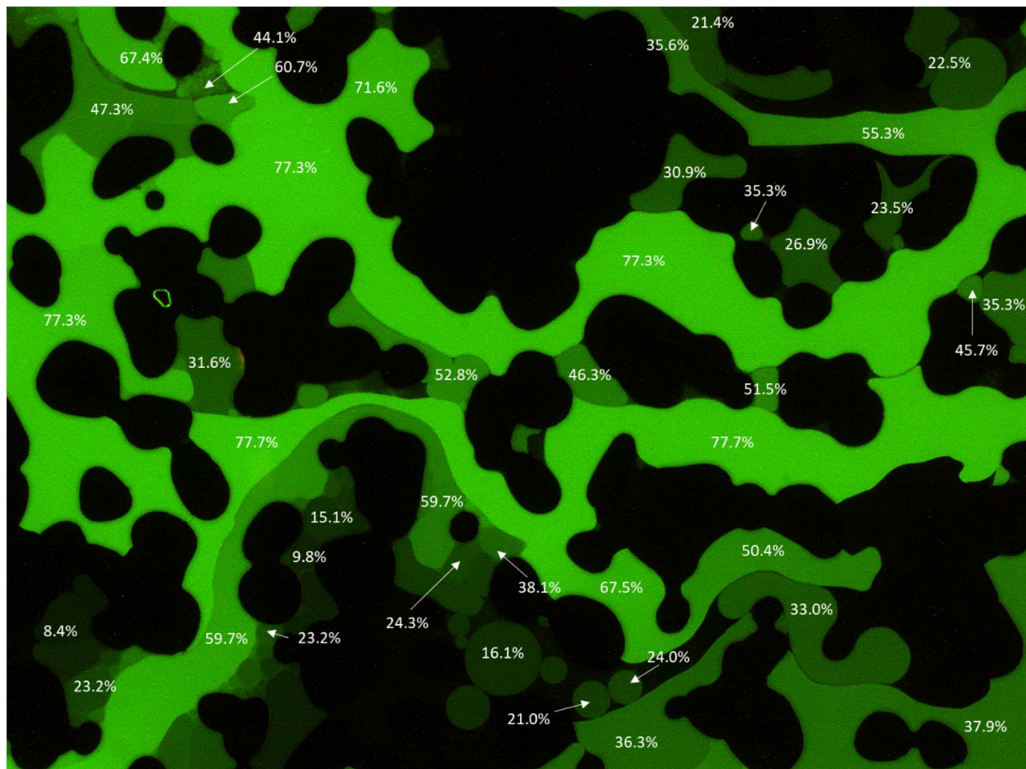


Figure 5-20 – Experiment 1.3 (4% NaCl) – Stage 06 – Mixing Analysis

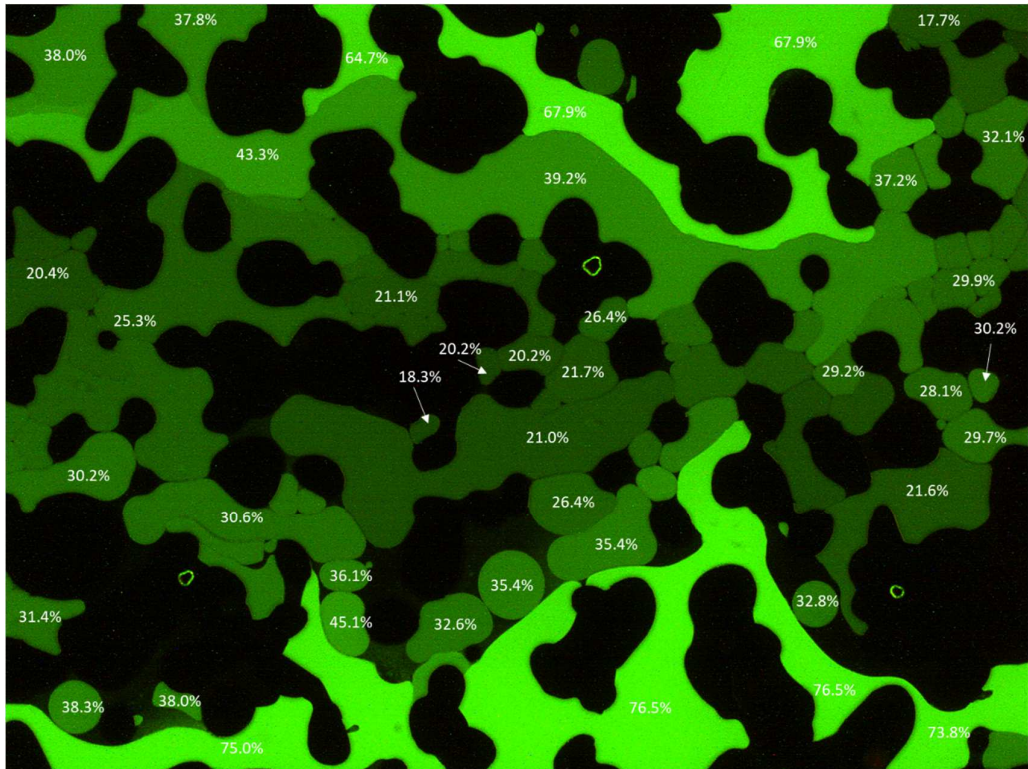


Figure 5-21 – Experiment 1.3 (4% NaCl) – Stage 12 – Mixing Analysis

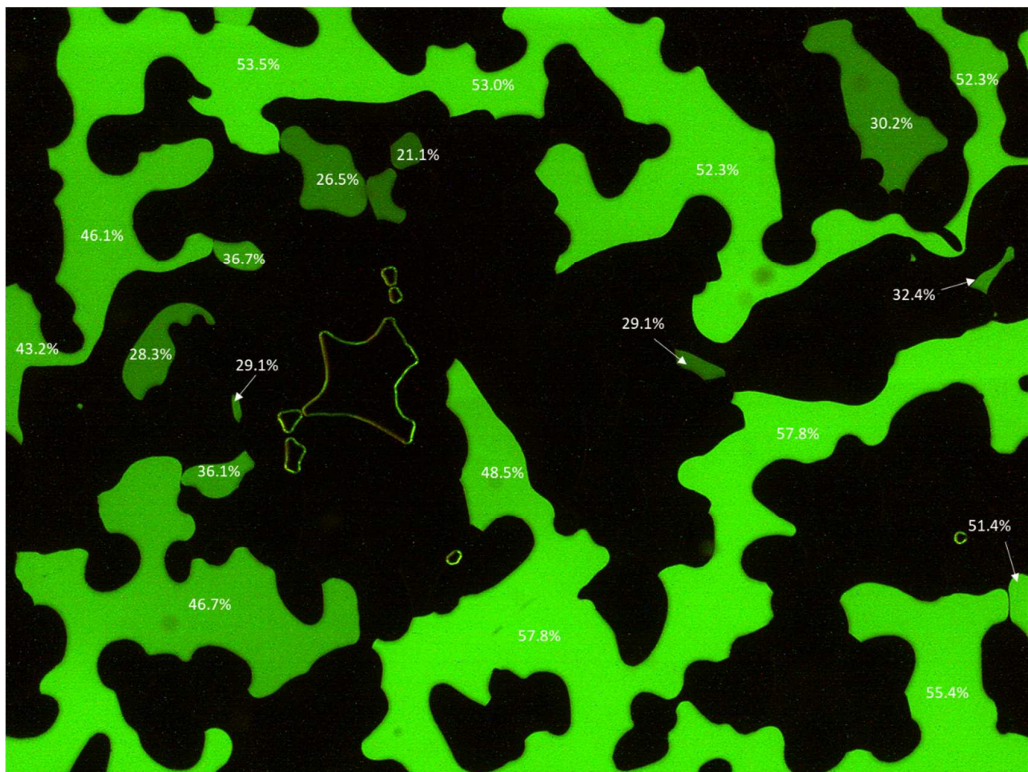


Figure 5-22 – Experiment 1.3 (4% NaCl) – Stage 06 – Mixing Analysis

### 5.1.2.5 Merged Image

The merged images underline the observations made previously in this chapter.

For Figure 5-23, even though the 1% NaCl-solution of experiment 3.1 avoided a substantial area, the areas which were penetrated showed an even distribution and a good displacement with some small oil droplets trapped in between. It is mandatory to note that during the stitching process, some data got lost in the upper left corner of the fluorescent image. This does not affect the result, since it did not cover an area of interest.

For the fluorescent merged images no correct scale can be added since LAS X was not able to assemble them correctly, leading to slight distortions. However, the porous network area should still be approximately 2 x 1 cm.

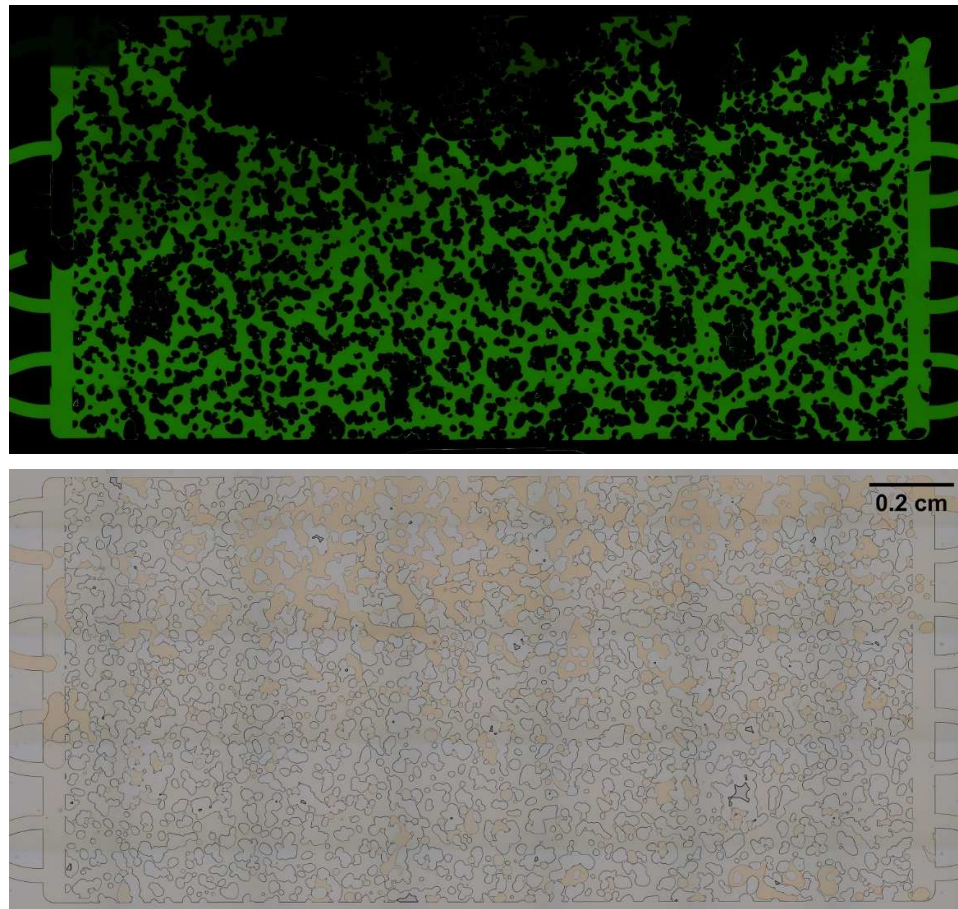
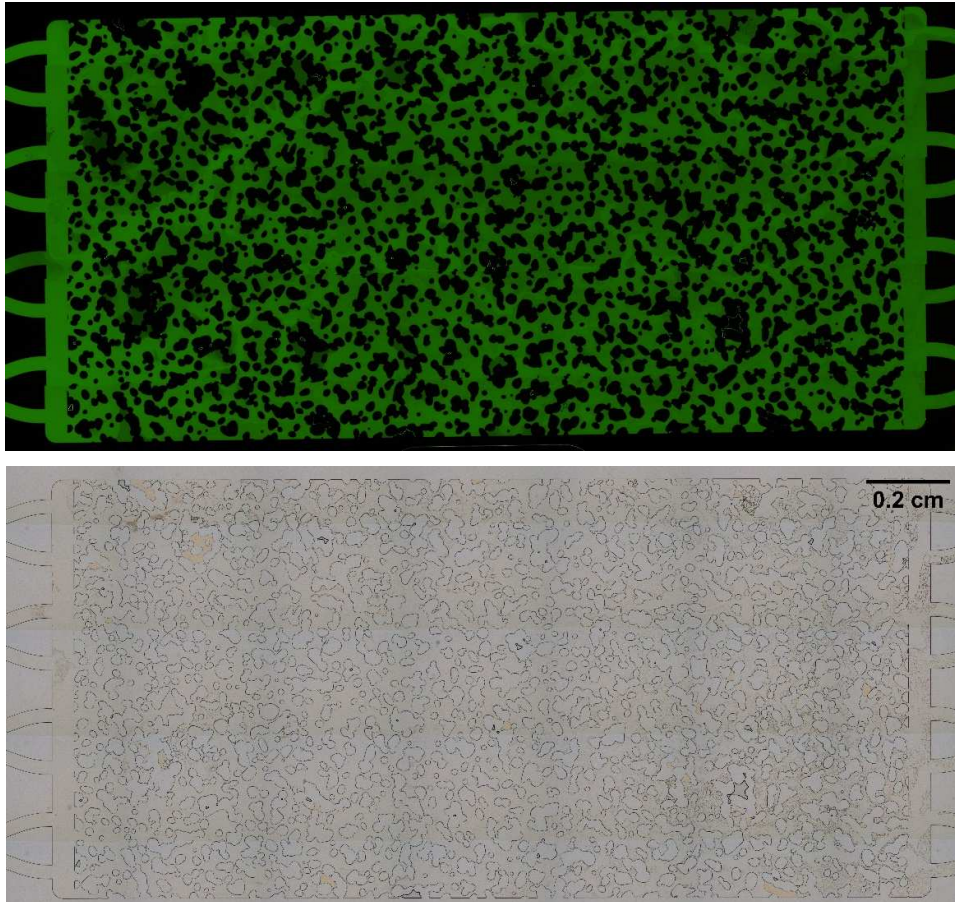


Figure 5-23 – Experiment 1.1 (1% NaCl) – Merged image: fluorescent ILL (top); normal ILL (bottom)

Experiment 1.2, which had the best result in all three stages, also shows the most efficient displacement in the merged image. Only small areas were bypassed and the solution was distributed evenly. One reason for the mostly uniform distribution could be due to the wettability state of the system. Since it is initially saturated with oil, under vacuum, we can

state that the micromodel is oil wet. Therefore, a film of oil could cover the surface of the pores which is bypassed by the aqueous solution, but is still thin enough to not influence the fluorescent illumination. Also a slight intensity variation can be seen in some areas of the micromodel, which can be explained by the gathering of small droplets.



*Figure 5-24 – Experiment 1.2 (2% NaCl) – Merged image: fluorescent ILL (top); normal ILL (bottom)*

Meanwhile, the 4% NaCl-solution showed a different behavior to both 1.1 and 1.2 experiments. Only some areas in the central area of the microfluidic chip were bypassed, which are surrounded by a mixture of oil and solution, which can be seen by the decrease in intensity. It also seems that the region near the inlet received a better distribution and the brown spaces in the bottom image of Figure 5-25 indicate a very small droplet size.

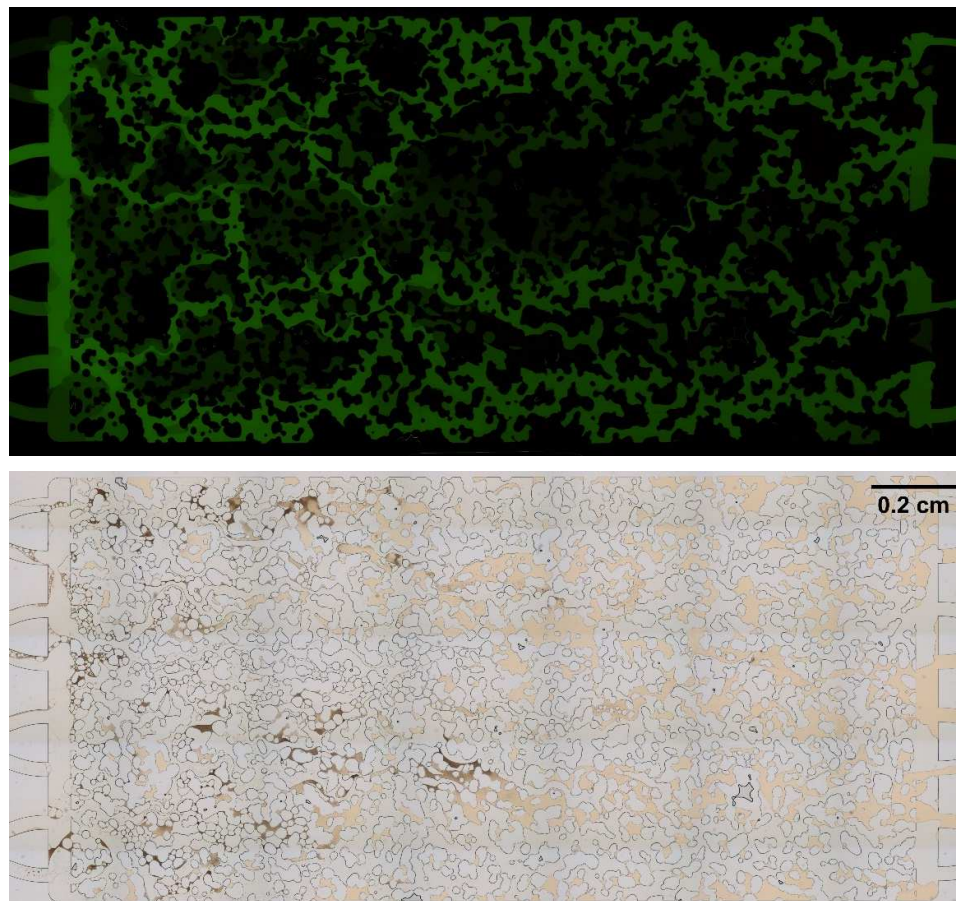


Figure 5-25 – Experiment 1.3 (4% NaCl) – Merged image: fluorescent ILL (top); normal ILL (bottom)

For some experiments the possibility exists, that the oil distribution changed due to trapped oil the near the inlet being mobilized. However, observation of this phenomenon during displacement was not possible, since the focus was on specific tiles and no merged images exist for this time being.

For over- and under-optimum, foam-like structures can be observed. Although, the term foam is typically used in respect to gas-surfactant flooding, the mechanisms seem to be applicable for surfactant flooding as well, when looking at the structure. They form plateau borders and lamellas, where the oil phase is enclosed. The absence of coalescence between the touching droplets can be explained by the formation of low-quality foams. The foam quality increases over time and distance, when more oil is solubilized and stabilized by the surfactants in the lamella.

These formations can be seen for all displacement experiments. However, the closer the solution is to optimum with ultra-low IFT, the presence of foam-like structures become rarer, since the foam starts to collapse. This can also be seen for experiment 1.2 (2% NaCl) which is the closest to optimum.

## 5.2 Characterization of Fluid System

### 5.2.1 Pendant Drop Method

During the implementation of the pendant drop method, it became apparent that the IFT could not be measured using this setup (See 4.2.1). The IFT was so low that the dispensing of decane could not be stopped and droplets escaped uncontrollably. Furthermore, the droplets started to spread out immediately when contacting the glass plate, making it impossible to measure. Despite the limitations of this method, it still shows that the IFT decreases with salinity by comparing Figure 5-26 (1% NaCl) to Figure 5-27 (2% NaCl) and states that the IFT is low in general which was expected.



Figure 5-26 – Experiment 3.1 (1% NaCl)

In Figure 5-27, a timeline of decane being dispensed in a 2% NaCl solution (experiment 3.2) can be seen, which visualizes the spreading behavior.



Figure 5-27 – Experiment 3.2 (2% NaCl) – Timeline from left to right

For experiment 3.3 (4% NaCl), no images could be taken since the needle was not visible due to the foggy appearance of the solution.

### 5.2.2 Spinning Drop Tensiometer

For the spinning drop tensiometer, we faced similar problems to the pendant drop method. Due to the low IFT and the formation of emulsion, no clear statement could be made. Although in the central and right image of Figure 5-28, IFT values of 1.86 mN/m and 0.22 mN/m could be

measured, these results should be considered with care and only be taken to state that the IFT is low, but not an exact value. We can see on the left image that emulsions started to oscillate around the left and right side of the droplet, which made the droplet's outlines hard to detect and distort the measurement.

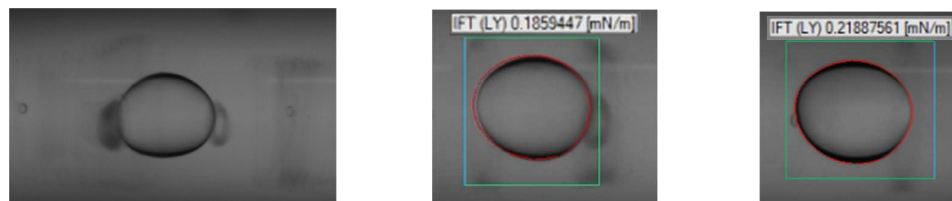


*Figure 5-28 – Experiment 4.2 (2% NaCl): 1000 rpm, 25.7°C*

For 4.3 (4% NaCl), no droplet could be formed and Figure 5-29 shows the experimental results. Emulsion started to form similarly around those shapes and tried to elongate towards the end of the capillary.

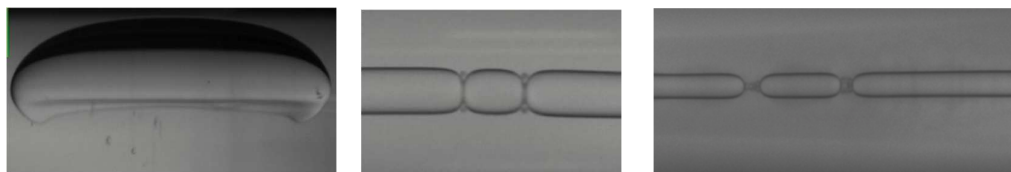


*Figure 5-29 – Experiment 4.3 – Attempts to measure IFT: 300 rpm, 25.9°C (left); 4000 rpm, 25.9°C (middle); 4000 rpm, 30°C (right)*

### 5.2.3 Phase Behavior

The primary purpose of the phase behavior experiments is to investigate the influence of fluorescein salt on the surfactant regarding salinity. As can be seen in Figure 5-30, the results for both look nearly identical. This states that the fluorescein salt does not visibly influence the surfactant and therefore can be used in the fluorescein microfluidic experiments.



Figure 5-30 – Phase Behavior Results: experiment 5.1 (left) to 5.6 (right)

Moreover, experiment 5.5 show under optimum conditions, while 5.6 shows over optimum salinity conditions. Consequently, we can assume that the near optimum salinity might lie between 2 and 4%.

# Chapter 6

## Conclusion

### 6.1 Summary

The objective of this thesis is to investigate the emulsion formation and behavior with varying salinities. For this reason, multiple experiments were executed:

- Fluorescent Intensity Analysis
- Fluorescent Displacement Analysis
- Pendant Drop
- Spinning Drop
- Phase Behavior

Foremost it had to be stated that the fluorescein sodium salt does not affect the surfactant and its behavior. Therefore, six different phase behaviors were executed, which can be split into two groups. Group one, where 100 mg of fluorescein salt on one-liter solution was added and group two, which was left untouched. The phase behaviors were placed into a shaker for 24 hours at a speed of 25 rounds per minute and then rested for three days. The result showed no visual differences between both groups. Even though static experiments, like phase behaviors, do not resemble dynamic experiments, like microfluidics, they still could be used to characterize the fluid behaviors. The 2% NaCl-solution showed an under optimum (Winsor Type I), whereas the 4% NaCl-solution showed an over optimum (Winsor Type II).

Furthermore, a fluorescent intensity analysis was performed to offer a statement about the ideal amount of fluorescein salt for best visibility during the microfluidic displacement experiments and to give a relationship between fluorescent intensity and fluorescein salt concentration. For this purpose, five different solutions were mixed with 2, 5, 10, 100 and 300 mg of fluorescein

salt dissolved in one liter of distilled water, which were then injected in a microfluidic chip with a physical rock pattern. 100 mg/l appeared to be the perfect amount since it is visible enough to be clearly distinguished from the background noise and not bright enough to over glow the grains. It also revealed a linear relationship between the mean gray value difference of the pore to the grain area and the fluorescein salt concentration, which could then be used to investigate the mixing of the emulsion.

The main experiments were conducted in a fully oil-saturated microfluidic chip, which was then displaced by the aqueous solution with varying salinity and added fluorescein salt. It could be observed that the 1% NaCl-solution bypassed prominent regions in the upper area of the chip; however, it showed a satisfactory overall displacement. The 4% NaCl-solution bypassed regions in the center of the chip, surrounded by dark green areas, indicating a partial mixture of oil and aqueous solution. Overall it can be stated that the solution with 2% salinity performed the best, considering displacement and fluid distribution. It was also discovered that even though not all dead-end pores were perfectly contacted, most of them were partly penetrated. This is in good agreement with recent research, which states that emulsions in the under optimum range are more desirable. Foam-like structures can be observed for all experiments, especially for under- (1% NaCl) and over-optimum (4% NaCl).

To accompany the emulsion characterization, two types of IFT tension measurements were executed with three different salinities: the pendant drop method and the spinning drop tensiometer. However, both of them failed to deliver precise results. For the pendant drop method, the IFT tension was so low that the droplet immediately spread once it came in contact with the borosilicate glass plate, making it impossible to measure. For the spinning drop tensiometer, the problem occurred that no distinct shape could be formed and although the program could conduct measurements, the results stay questionable. Emulsion phases oscillating around the droplet made it impractical to measure. Even though the IFT tension measurements gave no precise results, a general trend in IFT tension reduction could be observed comparing 1% salinity to 2% salinity.

## 6.2 Future Work

Since the formation of emulsions and surfactant flooding is a rather complex subject matter, I would like to bring some suggestions for future research topics:

- Cluster size distribution analysis implementing fluorescent salt
- Ultra-low IFT tension measurements
- Waterflooding followed by surfactant flooding implementing fluorescent salt
- Emulsion formation on a dead-end-pore microfluidic chip





# Chapter 7

## References

- Ahmad Kharrat (2018): Alkali-based Displacement Processes in Microfluidic Experiments: Advanced Statistical Analyses.
- Al-Yaari, M.; Hussein, I. A.; Al-Sarkhi, A.; Abbad, M.; Chang, F. (2015): Effect of water salinity on surfactant-stabilized water–oil emulsions flow characteristics. In *Experimental Thermal and Fluid Science* 64, pp. 54–61. DOI: 10.1016/j.expthermflusci.2015.02.001.
- Azam, Muhammad Rizwan; Tan, Isa M.; Ismail, Lukman; Mushtaq, Muhammad; Nadeem, Muhammad; Sagir, Muhammad (2013): Static adsorption of anionic surfactant onto crushed Berea sandstone. In *J Petrol Explor Prod Technol* 3 (3), pp. 195–201. DOI: 10.1007/s13202-013-0057-y.
- Broens, M.; Unsal, E. (2018): Emulsification kinetics during quasi-miscible flow in dead-end pores. In *Advances in Water Resources* 113, pp. 13–22. DOI: 10.1016/j.advwatres.2018.01.001.
- Buijse, Marten; Tandon, Kunj; Jain, Shekhar; Handgraaf, Jan-Willem; Fraaije, Johannes G. (2012): Surfactant Optimization for EOR Using Advanced Chemical Computational Methods.
- Chmeyx (2020): FUSION 200 TWO-CHANNEL SYRINGE PUMP. Available online at <https://www.chemyx.com/syringe-pumps/fusion-200/>, checked on 4/27/2021.
- Dataphysics: OCA 100 / 100Micro - Brochure.
- Dataphysics: SVT 20N - Brochure.
- Donaldson, Erle C.; Alam, Waqi (2008): Wettability and Production. In Erle C. Donaldson, Waqi Alam (Eds.): *Wettability*. Burlington: Elsevier Science, pp. 121–172.

- Fisher Scientific: Multi-Purpose Tube Rotator. Available online at [https://www.fishersci.de/shop/products/multi-purpose-tube-rotators/15524080?change\\_lang=true#?keyword=rotator](https://www.fishersci.de/shop/products/multi-purpose-tube-rotators/15524080?change_lang=true#?keyword=rotator), checked on 5/7/2021.
- Gerami, Alireza; Alzahid, Yara; Mostaghimi, Peyman; Kashaninejad, Navid; Kazemifar, Farzan; Amirian, Tammy et al. (2019): Microfluidics for Porous Systems: Fabrication, Microscopy and Applications. In *Transp Porous Med* 130 (1), pp. 277–304. DOI: 10.1007/s11242-018-1202-3.
- Gogoi, Sekhar; Gogoi, Subrata Borgohain (2019): Review on microfluidic studies for EOR application. In *J Petrol Explor Prod Technol* 9 (3), pp. 2263–2277. DOI: 10.1007/s13202-019-0610-4.
- Gold, Victor (2019): The IUPAC Compendium of Chemical Terminology. Research Triangle Park, NC: International Union of Pure and Applied Chemistry (IUPAC).
- Green, Don W.; Willhite, G. Paul (2008): Enhanced oil recovery. [4. Nachdr.]. Richardson, Tex.: Henry L. Doherty Memorial Fund of AIME Society of Petroleum Engineers (SPE textbook series, 6).
- Guzey, Demet; McClements, D. Julian (2006): Formation, stability and properties of multilayer emulsions for application in the food industry. In *Advances in colloid and interface science* 128-130, pp. 227–248. DOI: 10.1016/j.cis.2006.11.021.
- Hsu, Shao-Yiu; Zhang, Zhong-Yao; Tsao, Chia-Wen (2017): Thermoplastic Micromodel Investigation of Two-Phase Flows in a Fractured Porous Medium. In *Micromachines* 8 (2), p. 38. DOI: 10.3390/mi8020038.
- ImageJ: Versatile Wand Tool. Available online at <https://imagej.nih.gov/ij/plugins/versatile-wand-tool/index.html>, checked on 5/24/2021.
- Khan, Barkat Ali (2011): Basics of pharmaceutical emulsions: A review. In *Afr. J. Pharm. Pharmacol.* 5 (25). DOI: 10.5897/AJPP11.698.
- Kole, Subarna; Bikkina, Prem (2017): A parametric study on the application of microfluidics for emulsion characterization. In *Journal of Petroleum Science and Engineering* 158, pp. 152–159. DOI: 10.1016/j.petrol.2017.06.008.
- Lake, Larry W.; Johns, Russell; Rossen, Bill (2014): Fundamentals of Enhanced Oil Recovery. Richardson: SPE. Available online at <https://ebookcentral.proquest.com/lib/gbv/detail.action?docID=5139938>.

- Liu, Yichen; Li, Yongli; Hensel, Andreas; Brandner, Juergen J.; Zhang, Kai; Du, Xiaoze; Yang, Yongping (2020): A review on emulsification via microfluidic processes. In *Front. Chem. Sci. Eng.* 14 (3), pp. 350–364. DOI: 10.1007/s11705-019-1894-0.
- Ma, Kun; Cui, Leyu; Dong, Yezi; Wang, Tianlong; Da, Chang; Hirasaki, George J.; Biswal, Sibani Lisa (2013): Adsorption of cationic and anionic surfactants on natural and synthetic carbonate materials. In *Journal of colloid and interface science* 408, pp. 164–172. DOI: 10.1016/j.jcis.2013.07.006.
- Micronit: EOR Chip. Available online at [https://store.micronit.com/eor\\_chip.html](https://store.micronit.com/eor_chip.html), checked on 4/27/2021.
- Mostafa Borj (2017): Alkali-based Displacement Processes in Microfluidic Experiments: Application to the Matzen Oil Field.
- Nordiyana, M. S. W.; Khalil, Munawar; Jan, Badrul Mohamed; Ali, Brahim Si; Tong, Chong Wen (2016): Formation and Phase Behavior of Winsor Type III *Jatropha curcas*-Based Microemulsion Systems. In *J Surfact Deterg* 19 (4), pp. 701–712. DOI: 10.1007/s11743-016-1814-y.
- Ott, Holger; Kharrat, Ahmad; Borji, Mostafa; Arnold, Pit (2020): Fluid-phase topology of complex displacements in porous media. In *Phys. Rev. Research* 2 (2). DOI: 10.1103/PhysRevResearch.2.023240.
- Peter Bankhead (2014): Analyzing fluorescence microscopy images with ImageJ, May 2014.
- Pit Arnold (2018): Experimental investigation of interfacial tension for alkaline flooding.
- Schramm, Laurier Lincoln (2000): Surfactants. Fundamentals and applications in the petroleum industry. Cambridge, U.K, New York: Cambridge University Press. Available online at <http://site.ebrary.com/lib/alltitles/docDetail.action?docID=10438575>.
- Shell Chemicals: Ermodet Brochure.
- Sheng, James J. (2011): Modern chemical enhanced oil recovery. Theory and practice. Burlington, Mass.: Gulf Professional Publ.
- Sun, Chen; Guo, Hu; Li, Yiqiang; Song, Kaoping (2020): Recent Advances of Surfactant-Polymer (SP) Flooding Enhanced Oil Recovery Field Tests in China. In *Geofluids* 2020, pp. 1–16. DOI: 10.1155/2020/8286706.
- Sweeta Akbari (2018): Emulsion types, stability mechanisms and rheology: A review.

Vonnegut, Bernard (1942): Rotating Bubble Method for the Determination of Surface and Interfacial Tensions. In *Review of Scientific Instruments* 13 (1), pp. 6–9. DOI: 10.1063/1.1769937.

Winsor, P. A. (1948): Hydrotropy, solubilisation and related emulsification processes. In *Trans. Faraday Soc.* 44, p. 376. DOI: 10.1039/tf9484400376.

Zeppieri, Susana; Rodríguez, Jhosgre; López de Ramos, A. L. (2001): Interfacial Tension of Alkane + Water Systems †. In *J. Chem. Eng. Data* 46 (5), pp. 1086–1088. DOI: 10.1021/je000245r.

Zhang, Jun; Yan, Sheng; Yuan, Dan; Alici, Gursel; Nguyen, Nam-Trung; Ebrahimi Warkiani, Majid; Li, Weihua (2016): Fundamentals and applications of inertial microfluidics: a review. In *Lab on a chip* 16 (1), pp. 10–34. DOI: 10.1039/c5lc01159k.

# Appendix A

## Appendix Title

### A.1 Experiment List

Table 9 – List of all Experiments

FLUORESCENT DISPLACEMENT ANALYSIS						
#	Salinity	NaCl [g]	DI-W [g]	2-Butanol [g]	J13131 [g]	Fl-salt
1.1	1%	1 g	99.538 g	2 g	0.5 g	100 mg/l
1.2	2%	2 g	99.078 g			
1.3	4%	4 g	98.157 g			

FLUORESCCEIN INTENSITY ANALYSIS		
#	Fluorescein salt [mg/l]	Base
2.1	2	Distilled water
2.2	5	Distilled water
2.3	10	Distilled water
2.4	20	Distilled water
2.5	50	Distilled water
2.6	80	Distilled water
2.7	100	Distilled water
2.8	300	Distilled water

<b>PENDANT DROP</b>		
<b>#</b>	<b>Aqueous Phase</b>	<b>Droplet</b>
<b>3.1</b>	1% NaCl-solution	n-Decane 99.9% + Sudan II
<b>3.2</b>	2% NaCl-solution	n-Decane 99.9% + Sudan II
<b>3.3</b>	4% NaCl-solution	n-Decane 99.9% + Sudan II

<b>SPINNING DROP TENSIOMETER</b>				
<b>#</b>	<b>Aqueous Phase</b>		<b>Oleic Phase</b>	
<b>5.1</b>	1% NaCl-solution + Fluorescein salt	5 ml	n-Decane 99.9%	5 ml
<b>5.2</b>	2% NaCl-solution + Fluorescein salt	5 ml	n-Decane 99.9%	5 ml
<b>5.3</b>	4% NaCl-solution + Fluorescein salt	5 ml	n-Decane 99.9%	5 ml
<b>6.1</b>	1% NaCl-solution	5 ml	n-Decane 99.9%	5 ml
<b>6.2</b>	2% NaCl-solution	5 ml	n-Decane 99.9%	5 ml
<b>6.3</b>	4% NaCl-solution	5 ml	n-Decane 99.9%	5 ml

<b>PHASE BEHAVIOR</b>				
<b>#</b>	<b>Aqueous Phase</b>		<b>Oleic Phase</b>	
<b>5.1</b>	1% NaCl-solution + Fluorescein salt	5 ml	n-Decane 99.9%	5 ml
<b>5.2</b>	2% NaCl-solution + Fluorescein salt	5 ml	n-Decane 99.9%	5 ml
<b>5.3</b>	4% NaCl-solution + Fluorescein salt	5 ml	n-Decane 99.9%	5 ml
<b>6.1</b>	1% NaCl-solution	5 ml	n-Decane 99.9%	5 ml
<b>6.2</b>	2% NaCl-solution	5 ml	n-Decane 99.9%	5 ml
<b>6.3</b>	<b>4% NaCl-solution</b>	<b>5 ml</b>	<b>n-Decane 99.9%</b>	<b>5 ml</b>

## A.2 Fluorescein Salt Concentration

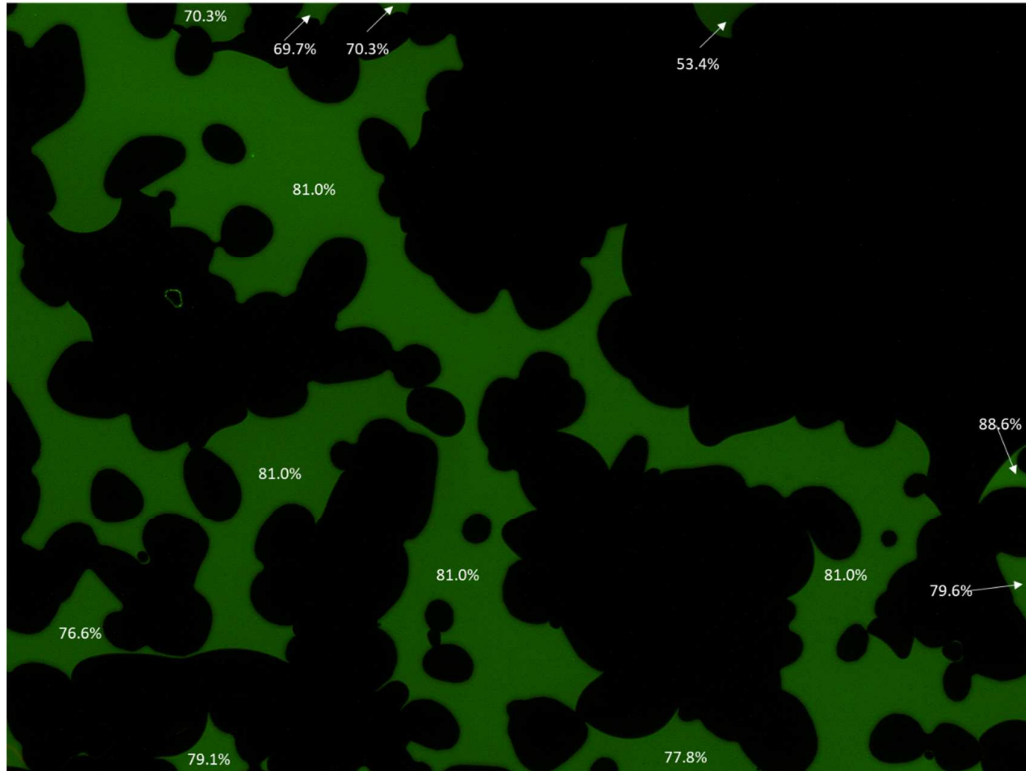


Figure 7-1 – Experiment 1.1 (1% NaCl) – Stage 06 – Mixing Analysis

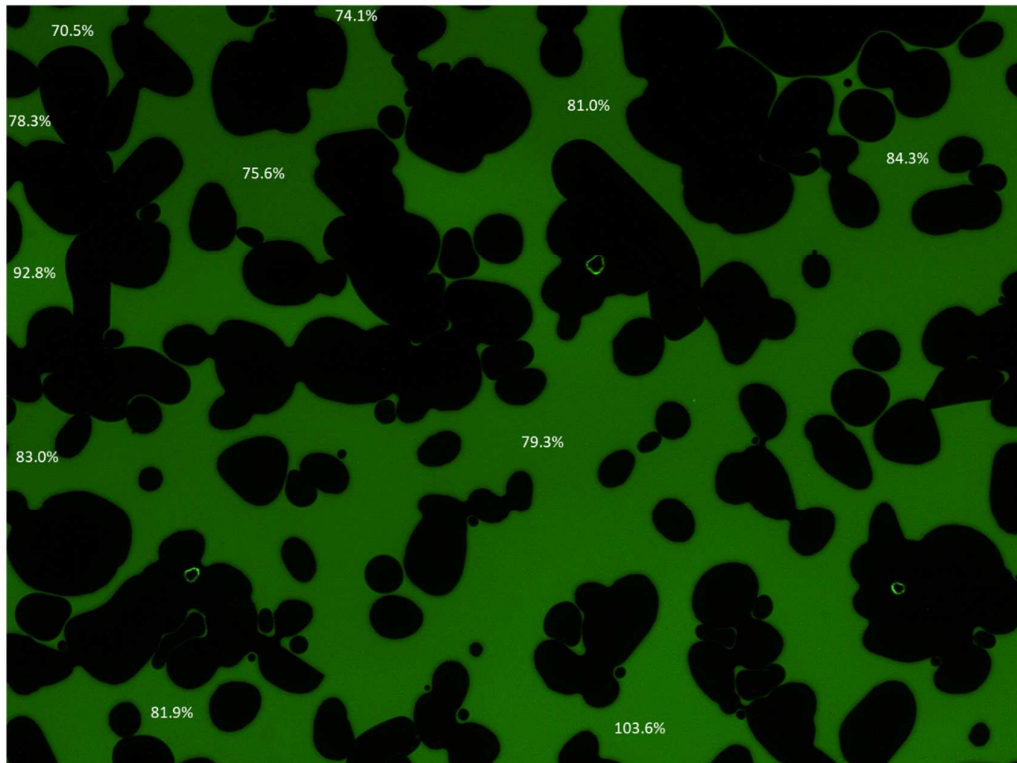
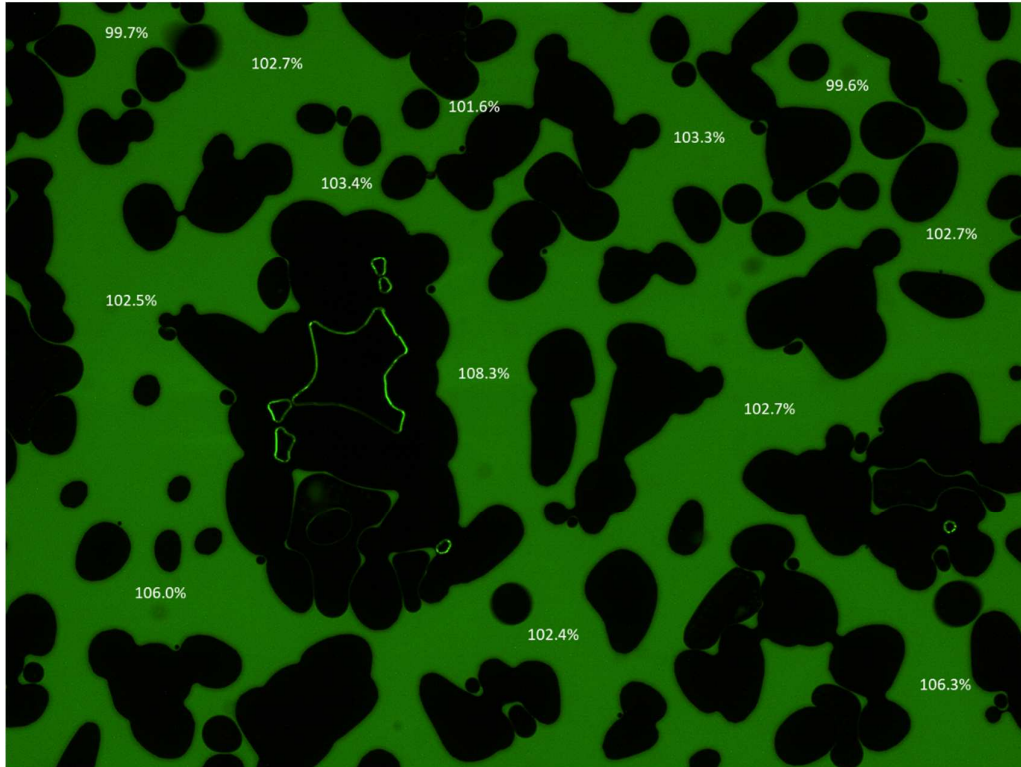


Figure 7-2 – Experiment 1.1 (1% NaCl) – Stage 12 – Mixing Analysis



*Experiment 1.1 (1% NaCl) – Stage 28 – Mixing Analysis*